ACS APPLIED NANO MATERIALS

www.acsanm.org Article

Microwave Synthesis of Gold Nanoparticles in Poly(Ethylene Glycol)-Based Hydrogels for Drug Delivery

Alessandro Molinelli, Julián Guacaneme Sánchez, Andrea Schirato, Francesco Briatico Vangosa, Margherita Maiuri, and Filippo Rossi*

Cite This: *ACS Appl. Nano Mater.* 2026, 9, 5067−5083 Read Online

ACCESS | Metrics & More | Article Recommendations | Supporting Information

ABSTRACT: Nanocomposite hydrogels incorporating gold nanoparticles (AuNPs) have garnered significant interest in biomedical and materials science thanks to the synergistic advantages resulting from the integration of the two systems. However, their fabrication typically involves multistep procedures that may alter the physicochemical features of the final platform, limiting their reproducibility and translational potential. In this study, we report a facile and fast one-pot synthesis for *in situ* formation of AuNPs within an agarose-carbomer-poly(ethylene glycol) (AC-PEG) hydrogel, eliminating the need for multistep nanocomposite assembly. The synthesis is carried out through microwave irradiation, leading to fast and homogeneous heating with a short reaction time (3 min). PEG simultaneously acts as Au precursor reducing agent and, jointly with carbomer, a stabilizer of the produced AuNPs against salt-induced aggregation. The role of solution pH and $HAuCl_4$ concentration is assessed by independently varying the parameters, respectively, in the ranges 6−11 and 0.25−2.27 mM. Postsynthetic NaOH addition, in a concentration between 12 and 15 mM, demonstrates to further improve the sample uniformity and the synthesis outcomes. The produced AuNPs are characterized by narrow UV−vis spectra, sizes around 15−20 nm, better sphere-like shapes, and improved size distributions (PdI ∼ 0.1), compared to the case without NaOH addition. The internal microstructure of AuNPs/AC-PEG nanocomposites is preserved, compared to pristine hydrogel, while AuNPs exhibit concentration-dependent swelling and viscoelastic behavior. Finally, drug release tests under laser irradiation demonstrate the light-responsiveness of the system, resulting in improved cumulative release (∼80%) of a small hydrophobic drug mimetic (FITC) when subjected to 10 min ON-OFF irradiation cycles for 2 h. This facile and rapid method enables the direct formation of plasmonic nanocomposite hydrogels with tunable properties, opening future routes for responsive system fabrication in biomedical and other applications.

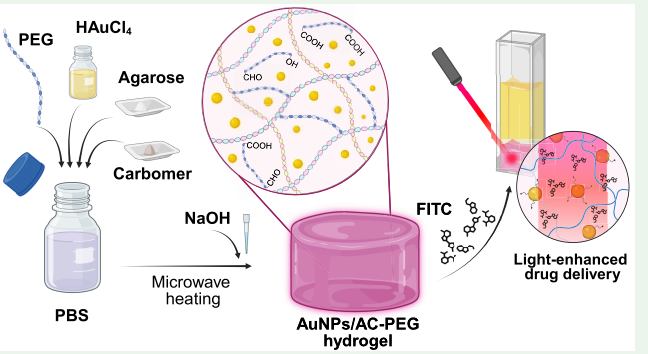

KEYWORDS: *gold nanoparticles, one-pot synthesis, nanocomposite hydrogel, drug delivery, laser irradiation, stimuli-responsiveness*

1. INTRODUCTION

Thanks to their unique optical and photothermal properties, plasmonic nanoparticles have gained broad interest across several fields, including nanomedicine, biotechnology, optics, catalysis, and material science.[1−3] The response of these metallic nanostructures to light originates from their electronic configuration, and it is governed by the localized surface plasmon resonance (LSPR) phenomenon, which is highly sensitive to the nanoparticles' surface-to-volume ratio, size, shape, and environment.[4,5] The design of hybrid nanocomposite materials, by combining plasmonic metal nanoobjects, typically gold nanoparticles (AuNPs), with organic supporting materials, such as hydrogels, has offered superior advantages in the field of drug delivery,[6−9] tissue engineering,[10,11] cancer treatment,[12,13] and hyperthermia.[14] In this perspective, hydrogels are highly attractive platforms for nanocomposites fabrication thanks to the excellent biocompatibility, biodegradability, and porosity, which make them relevant for several biomedical applications.[15,16] The inclusion of AuNPs to form hydrogel nanocomposites provides advantages to both the single components, by endowing the hydrogel with stimuli-responsiveness and improved mechanical properties, while providing a support for AuNPs, protecting them from the external environment.[9,17] The nanocomposite formulation is usually obtained by (i) dispersion of AuNPs before the hydrogel assembly or (ii) inclusion of AuNPs within the already formed polymeric support. However, both these strategies may alter the final composite systems' physicochemical properties.[18] AuNPs synthesis has been carried out mainly

Received: December 26, 2025
Revised: March 4, 2026
Accepted: March 5, 2026
Published: March 11, 2026

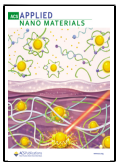

https://doi.org/10.1021/acsanm.5c05814
ACS Appl. Nano Mater. 2026, 9, 5067−5083

by employing bottom-up approaches, with the Turkevich method being the "gold standard" for spherical nanoparticles.[19−21] The nanoparticles' final properties can be tuned by modulation of the synthetic method and by modification of surface decoration, enabling precise control over size, colloidal stability, charge, optical behavior, and biological interactions.[5,22] A multitude of alternative AuNPs synthetic approaches have been investigated, including two-step seed-growth methods,[23,24] substitutional reducing agents, e.g., salts,[25,26] polymers,[27−31] amino acids,[32] polysaccharides,[33] bio-organisms,[22,34] and use of alternative solvents.[35,36]

However, the formation of nanocomposite materials requires multiple steps, including AuNPs synthesis and purification, surface functionalization, and then composite system assembly, posing severe limitations in preventing the alteration of final system properties, thus hindering their translational applications. Moreover, the use of some chemicals, such as sodium borohydride or cetyltrimethylammonium bromide (CTAB),[37−39] poses severe environmental and safety concerns, limiting AuNPs downstream biomedical use. In this framework, *in situ* synthesis of AuNPs has emerged as an alternative to create nanocomposites, where the nanoparticles are directly formed within the supporting material from the reduction of the gold precursor salt.[40] This strategy not only offers procedural advantages, but it could also provide control over the *in situ* growth process of anisotropic AuNPs within hydrogels.[41] To date, many of the proposed strategies employ externally added mild or strong reducing agents, either to the pre-gel solution or the already formed hydrogel, in the presence of the gold precursor salt or Au seeds.[18,42−44] However, only limited scenarios have been presented using a one-pot synthesis of AuNPs hydrogel nanocomposite, where the polymeric hydrogel constituents themselves act concurrently as reducing and stabilizing agents for AuNPs.[29,45−47] Additionally, considering the high importance of ionic solvents in biomedical applications, e.g., phosphate saline buffer (PBS), only a few examples of one-pot AuNPs synthetic methods have been proposed in PBS to the best of our knowledge,[48] due to the exerted salt effect, hindering the AuNPs stability.[49] In this regard, inspired by the ability of poly(ethylene glycol) (PEG) to act as a reducing agent for inorganic salts,[50,51] we propose an alternative method for one-pot synthesis of AuNPs nanocomposite hydrogel without the use of any organic solvents, catalysts, and tensides, where hydrogel formation and *in situ* AuNPs synthesis simultaneously occur. To this end, a polymer mixture containing carbomer and PEG (AC-PEG) in PBS was employed as the reactive solution for AuNPs synthesis by the addition of $HAuCl_4$ as gold precursor.

The reaction was carried out under microwave heating, where PEG and carbomer, already required as a structural component of the hydrogel network, respectively, provided the Au precursor reducing environment and helped in stabilization of AuNPs in the highly ionic solvent. The reaction did not require additional reducing agents or multiple-step synthesis, representing a facile and rapid strategy to obtain stable and well-dispersed AuNPs within a polymeric solution. The nanoparticles' properties were investigated as a function of different synthetic parameters (pH and $HAuCl_4$ concentration), to determine the best conditions yielding spherical, small, and monodispersed AuNPs. Additionally, the role of NaOH was investigated in terms of both pH modifier and catalytic agent for the reaction. The influence of NaOH addition time and amount was studied to afford the best properties of the final synthetic product. Then, the *in situ* hydrogel nanocomposite formation was achieved when agarose was added to the reactive mixture, through microwave-assisted polycondensation between the hydroxyl and carboxylic groups of the polymeric components. Microwave irradiation was selected to facilitate the homogeneous and fast heating of the reactive solution to improve reproducibility while minimizing the reaction times and solvent evaporation. The resulting nanocomposites, formulated with different AuNPs concentrations, were characterized in terms of swelling, morphology, rheological properties, and drug delivery performances. Finally, exploiting the AuNPs photothermal properties, laser irradiation tests were performed to study the light-assisted drug delivery enhancement using a drug mimetic. This strategy enabled the direct one-pot fabrication of responsive hydrogel-nanoparticle composites suitable for light-enhanced drug release, distinguishing the present system from previously reported platforms.

2. MATERIALS AND METHODS

2.1. Materials

Tetrachloroauric (III) acid trihydrate ($HAuCl_4{\cdot}3H_2O$, 99%), hydrochloric acid (HCl, >37%), sodium citrate tribasic dihydrate (NaCitrate, ≥99%), sodium hydroxide (NaOH, ≥97%), Dulbecco phosphate buffer (PBS), glycerol (≥98.5%), fluorescein isothiocyanate isomer I (FITC, ≥90%), fluorescein sodium salt (Fluo), poly(ethylene glycol) ($PEG_{2000,}$ MW = 2000 Da), poly(ethylene glycol) monomethyl ether (PEG_{5000}-CH_3, MW = 5000 Da), thioglycolic acid (TGA, 98%), and ultrapure water were all purchased from Sigma-Aldrich. Agarose (MW = 200 kDa) was purchased from Invitrogen, USA. Carbomer 974P (MW = 1 MDa) was purchased from Fargon, Netherlands. Deionized water (18.2 MΩ) was obtained from a Millipore Milli-Q purification unit. All chemicals were used without further purification, unless otherwise specified.

2.2. Microwave-Assisted One-Pot AuNPs Synthesis in AC-PEG Solution

All of the glassware has been carefully washed with aqua regia (3:1 v/v HCl/HNO_3 solution) and extensively rinsed with water before use. The polymer solution was obtained by dissolving carbomer 974P, PEG_{2000}, and glycerol in PBS, at final concentrations of 5, 60, and 12.6 mg/mL, respectively. The pH of the solution was adjusted to fixed values (ranging from 6 to 11) using 1 M NaOH. Then, 3 mL of the polymeric solution was preheated to 50 °C through electromagnetic stimulation at 500 W. Afterward, fixed amounts (from 30 to 300 μL) of a 25 mM $HAuCl_4$ solution were added under stirring, until reaching a transparent solution.

The reaction mixture was heated to 80 °C under electromagnetic stimulation at 500 W for 3 min, the time needed until the solution turned from transparent to red/violet. The obtained colloidal AuNPs solution was allowed to cool to room temperature and stored at 4 °C.

2.3. Microwave-Assisted One-Pot AuNPs Synthesis in Polymeric Solution with Postsynthesis NaOH Addition

All the glassware has been carefully washed with aqua regia (3:1 v/v HCl/HNO_3 solution) and extensively rinsed with water before use. The polymer solution was obtained by dissolving carbomer 974P, PEG_{2000}, and glycerol in PBS, at a final concentration of 5, 60 and 12.6 mg/mL, respectively. The pH of the solution was adjusted to 6.5 using 1 M NaOH. Then, 3 mL of the polymeric solution was preheated to 50 °C through electromagnetic stimulation at 500 W. Afterward, fixed amounts (from 30 to 300 μL) of a 25 mM $HAuCl_4$ solution were added under stirring, until reaching a transparent solution. The reaction mixture was heated to 80 °C under electromagnetic stimulation at 500 W for 3 min, the time needed until the solution turned from transparent to red/violet. After 60 s, a

https://doi.org/10.1021/acsanm.5c05814
ACS Appl. Nano Mater. 2026, 9, 5067−5083

fixed amount of 1 M NaOH (in the range 10−60 μL) was added to the reactive solution under vigorous stirring. The obtained colloidal AuNPs solution was allowed to cool down to room temperature and stored at 4 °C.

2.4. AuNPs Characterization

2.4.1. Transmission Electron Microscopy Analysis. The size and morphology of the synthesized AuNPs in solution were confirmed by transmission electron microscopy (TEM). Samples were prepared by placing a 10-μL drop of AuNPs dispersion on a Lacey carbon-coated copper TEM grid (400 mesh) and drying overnight to evaporate the solvent. Digital images were acquired by using a CM200FEG Philips microscope at 200 kV. Particle size analysis was performed for each sample using ImageJ software with a statistically representative population of nanoparticles. TEM images were scale-calibrated and processed via automated particle analysis to extract Feret diameters and circularity, applying pixel filters to exclude noise and aggregates.

Then, mean diameter, standard deviation, polydispersity index, and size distributions were obtained from mathematical calculations, and data were fitted using a log-normal model.

2.4.2. UV−Vis Analysis. The optical properties of the synthesized AuNPs in solution were evaluated by using a Jasco-630 UV−vis spectrophotometer over a range of wavelengths from 350 to 1000 nm. 1 mL of the sample was placed in 1 cm optical length plastic disposable cuvettes, and the analysis was performed at 25 °C.

2.4.3. Inductively Coupled Plasma Optical Emission Spectroscopy (ICP-OES) Analysis. The Au concentration of the synthesized AuNPs was determined by inductively coupled plasma optical emission spectroscopy (Optima 8300 ICP-OES, PerkinElmer, Shelton, CT, USA) using around 1 mL of concentrated sample.

2.5. AC-PEG Hydrogel Formulation

The hydrogel formulation was adapted from a previous protocol.[52] Briefly, carbomer 974P, PEG_{2000}, and glycerol, at final concentrations of 5, 60, and 6.3 mg/mL, respectively, were dissolved in PBS under stirring at room temperature. The pH of the solution was adjusted to 7.4 by using 1 M NaOH. Agarose was added to the prepared solution (at a 5 mg/mL concentration), and the mixture was heated up to 80 °C through electromagnetic stimulation at 500 W power, in a ratio of 1 min per mL of polymeric solution. When the reaction was terminated, the pre-gel solution was diluted in a 1:1 v/v ratio with PBS. After mixing, 0.5 mL of the solution was transferred to 1 cm diameter cylindrical molds, where the sol−gel transition was carried out.

2.6. AuNPs *In Situ* Synthesis in AC-PEG Hydrogel

All the glassware has been carefully washed with aqua regia (3:1 v/v HCl/HNO_3 solution) and extensively rinsed with water before use. Carbomer 974P, PEG_{2000}, and glycerol were dissolved in PBS under stirring at room temperature, at concentrations of 5, 60, and 12.6 mg/mL, respectively. The pH of the solution was adjusted to 6.5 using a 1 M NaOH. 3 mL of the solution was heated to 50 °C through electromagnetic stimulation at 500 W power, after which different amounts of 25 mM $HAuCl_4$ (from 30 to 300 μL) were added under stirring until obtaining a transparent mixture. Successively, agarose was added to the reaction mixture (in a concentration of 5 mg/mL), which was heated through electromagnetic stimulation at 500 W in a ratio of 1 min per mL of polymeric solution, after which the reaction mixture turned from transparent to violet. After 60 s, NaOH was added at a final concentration of 14.2 mM under vigorous stirring. Before the sol−gel transition, the pre-gel solution was diluted in a 1:1 v/v ratio with PBS, and 0.5 mL was transferred to 1 cm diameter cylindrical molds.

2.7. AC-PEG and AuNPs/AC-PEG Characterization

2.7.1. Fourier Transform Infrared Spectroscopy Analysis. Fourier transform infrared spectroscopy (FT-IR) analysis of the hydrogels synthesized was performed by using an Agilent Cary 630 spectrometer from Agilent Technologies. The spectra were recorded at room temperature in the 650−4000 cm^{-1} range with 4 cm^{-1} resolution and 64 scans/spectra under dry nitrogen conditions. The spectra were processed and reported with baseline correction and a reversed y-axis.

2.7.2. Differential Scanning Calorimetry Analysis. Differential scanning calorimetry (DSC) analysis was performed by using a Mettler Toledo DSC Polymer machine (Mettler Toledo, Greifensee, Switzerland) calibrated with zinc and indium standards. The analysis was performed on freeze-dried samples.

The heating rate was set to 10 °C min^{-1}, in a temperature window ranging between −20 and 100 °C, and the analysis was performed under nitrogen flow.

2.7.3. Swelling Kinetics Test. The hydrogel water reabsorption kinetics were tested at room temperature with cylindrical-shaped hydrogels (10 mm diameter, 0.5 mL volume), formulated as described above, and freeze-dried. After the initial mass (w_0) was evaluated, each hydrogel was soaked with 5 mL of Milli-Q water. At specific time points, the water was removed, and the mass of the hydrogel (w_t) was recorded. The hydrogels were covered again with 5 mL of freshly added Milli-Q water. For each time point recorded, the percentual mass swelling ratio (SR) was evaluated with eq 1, where w_t and w_0 are the mass of the swollen hydrogel at time t and the initial hydrogel mass at time zero, respectively.

$$\mathrm{SR}[\%] = \frac{w_t - w_0}{w_0} \times 100 \tag{1}$$

2.7.4. Rheological Analysis. Rheological properties were investigated by performing oscillatory measurements with an Anton Paar MCR 502 rheometer equipped with a parallel plate measuring system (diameter: 25 mm, plate−plate distance: 1 mm) at a fixed temperature of 25 °C. The samples were formulated in cylindrical shape (10 mm diameter, 1 mL volume). Briefly, amplitude sweep tests were carried out to determine the linear viscoelastic (LVE) region limit, the storage modulus (G'), and the loss modulus (G'') of the hydrogel, varying the shear strain amplitude in logarithmically spaced steps ranging from 0.01 to 100% at a fixed frequency of 10 rad/s. Frequency sweep tests were performed to describe the hydrogel viscoelastic behavior in the linear range by variation of the frequency in logarithmically spaced steps ranging from 0.1 to 100 rad/s, using a constant shear strain amplitude of 0.4% (within the sample LVE region).

2.7.5. Scanning Electron Microscopy Analysis. Scanning electron microscopy (SEM) analysis was carried out on gold sputtered cylindrical-shaped (1 cm diameter, 0.5 mL volume) dry samples to determine the internal morphology of the hydrogel using a Zeiss Evo50 with an EDS Bruker Quantax 200 microscope. The samples were formulated and immediately frozen at −80 °C and then freeze-dried for the analysis.

2.8. Drug Delivery Tests from AuNPs/AC-PEG Hydrogel

Drug release tests were performed on both AuNPs-containing and blank samples. Briefly, the hydrogels were formulated as previously described and encapsulated with different molecules by 1:1 v/v dilution before sol−gel transition with either BSA-FITC (2 mg/mL), FITC (0.5 mg/mL), or fluorescein (1 mg/mL) solutions in PBS. The hydrogels (0.5 mL volume, 1 cm diameter cylindrical shape) were covered with 2 mL of PBS in Corning 24 multiwell plates at 37 °C. At specific time intervals, 1 mL of the release media was withdrawn and replaced with 1 mL of PBS. The withdrawn samples were analyzed at room temperature using a Tecan microplate reader at a fixed wavelength corresponding to the fluorophore absorptions (λ = 495 nm for BSA-FITC, λ = 495 nm for FITC, and λ = 485 nm for fluorescein). The cumulated drug release [%] was calculated by evaluating the drug released through a calibration curve obtained using Lambert−Beer law, which correlates the read-out absorbance to the sample concentration, reported in Figure S1, Supporting Information.

https://doi.org/10.1021/acsanm.5c05814
ACS Appl. Nano Mater. 2026, 9, 5067−5083

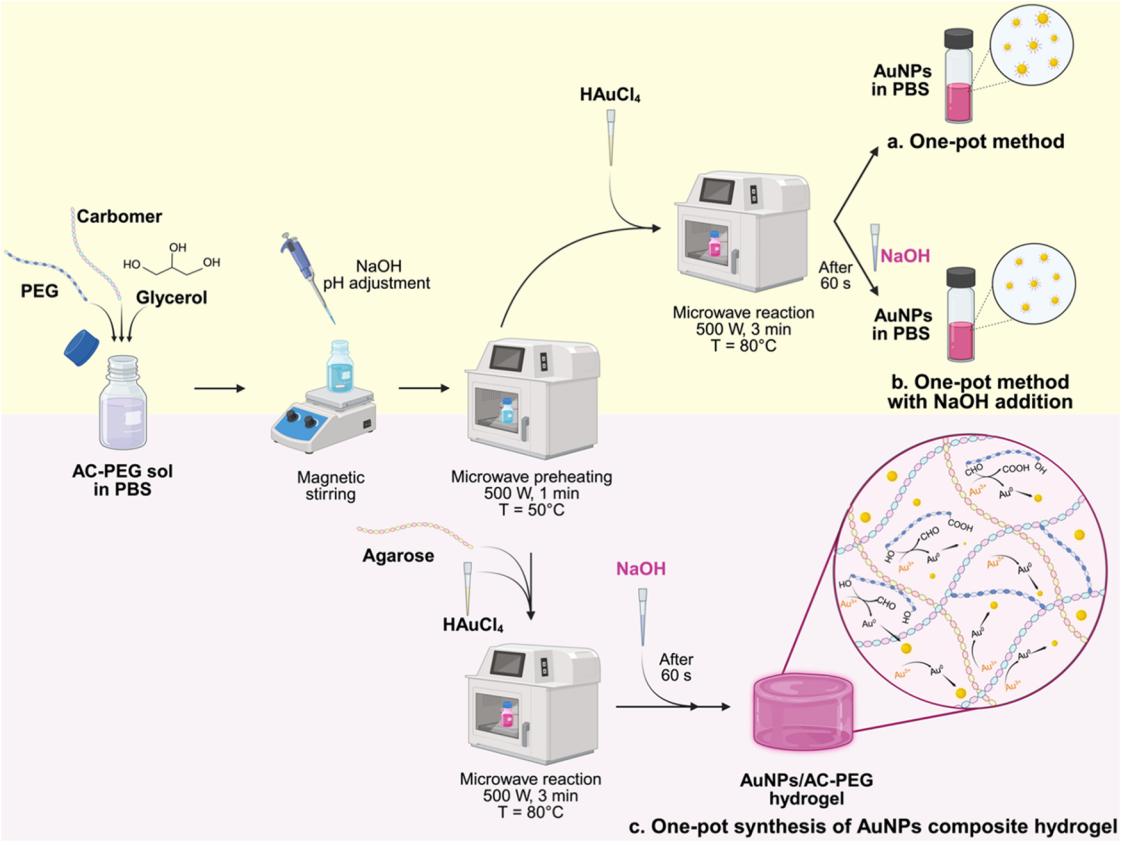

Figure 1. Schematic illustration of the synthetic strategies for AuNPs formation in AC-PEG solution, respectively representing: (a) one-pot method, (b) one-pot method modified with NaOH postsynthetic addition to AuNPs, and (c) one-pot method for the *in situ* synthesis of AuNPs composite AC-PEG hydrogels. Image created with Biorender.com.

2.9. Laser-Assisted Drug Delivery Tests from AuNPs/AC-PEG Hydrogel

FITC was used as a mimetic to study the drug release kinetics under laser irradiation in AuNPs-containing hydrogels. Briefly, the hydrogels were prepared as previously described and encapsulated with FITC by 1:1 v/v dilution before the sol−gel transition with a 1 mg/mL FITC solution in PBS.

0.5 mL portion of hydrogel was formulated in a 4.5 mL volume polystyrene Fisherbrand disposable cuvette and placed in a holder of a self-designed setup for laser irradiation. Each hydrogel was covered with 1 mL PBS and subjected to multiple 10 min laser irradiations at different times using a 632 nm continuous wavelength (CW) helium−neon laser diode at a power of 5 mW. At specific time points during the release test, 0.5 mL of the release medium was withdrawn, after volume homogenization by gentle mixing, and replaced with 0.5 mL of PBS. The withdrawn samples were analyzed at room temperature using a Tecan microplate reader at a fixed wavelength (corresponding to the fluorophore absorption, λ = 495 nm for FITC). The cumulated FITC release [%] was evaluated by calculating the drug released through a calibration curve, obtained using the Lambert−Beer law, which correlates the read-out absorbance to the sample concentration.

2.10. Statistical Analysis

The experimental data were analyzed using analysis of variance (ANOVA) with Tukey post hoc tests for comparison of different groups and evaluation of the p-value. Statistical significance was set to p value <0.05. Results were presented as mean value ± standard deviation, * $p < 0.05$; ** $p < 0.01$; *** $p < 0.001$, and **** $p < 0.0001$.

3. RESULTS AND DISCUSSION

For the *in situ* synthesis of AuNPs inside the hydrogel, a microwave-assisted reaction has been carried out using PEG. With the final aim of producing a hydrogel composite system with AuNPs, while maintaining the formulation parameters, microwave-irradiation heating was employed as an alternative to conventional heating. The feasibility was assessed within the Turkevich reduction protocol, obtaining AuNPs with comparable morphology, LSPR, and size distribution (Figure S2, Supporting Information). Microwave heating minimizes reaction times and improves reproducibility while limiting uncontrolled solvent evaporation. PEG is a well-known reducing agent of the gold and silver precursor, as found in previous studies.[50,53] Under such conditions, oxidation is expected to primarily involve terminal hydroxyl groups, leading to the formation of aldehyde and carboxylic PEG terminal groups, as reported for polyol-based reduction processes (Figure S3, Supporting Information).[54] The synthetic parameters have been optimized in the pre-gel polymer solution, before switching to the AuNPs synthesis *in situ* within the hydrogel. The reaction solvent consisted of a polymeric mixture, whose main components were PEG_{2000} and carbomer (AC-PEG sol) dissolved in PBS, selected from previous studies.[52] PBS can prevent gelification of the polymeric mixture, driven by the carbomer self-assembly in alkaline conditions.[55,56] To the best of our knowledge, few AuNPs synthetic methods have been previously proposed in PBS-based solutions,[48] due to aggregation arising from the salt effect. However, PBS represents a crucial factor in AC-PEG

https://doi.org/10.1021/acsanm.5c05814
ACS Appl. Nano Mater. 2026, 9, 5067−5083

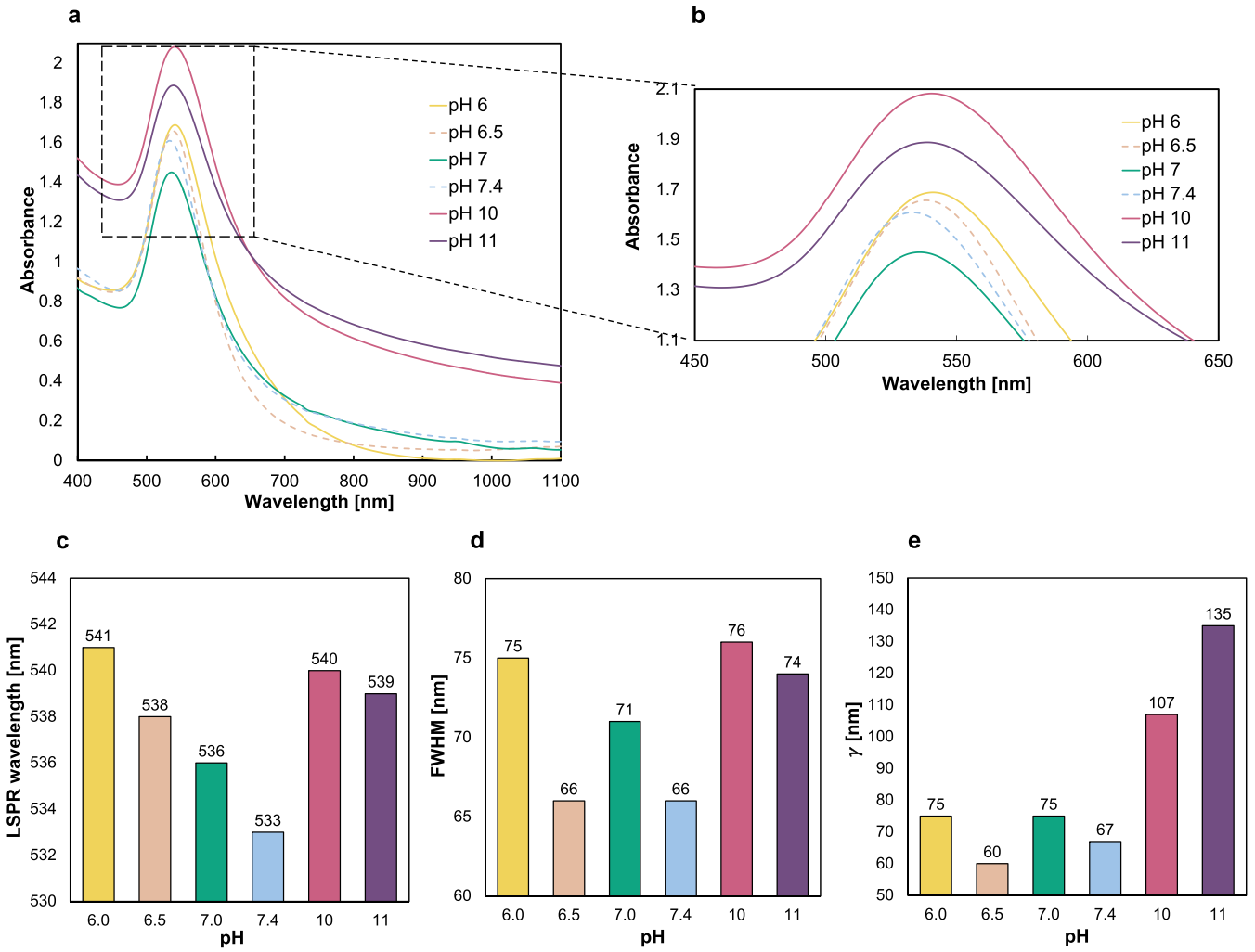

Figure 2. (a) UV−vis spectra of AuNPs synthesized in AC-PEG sol at PEG/$HAuCl_4$ = 60 with initial pH 6 (yellow), pH 6.5 (green), pH 7 (aquamarine), pH 7.4 (light blue), pH 10 (purple), pH 11 (violet); (b) UV−vis spectra magnification; (c) LSPR peak wavelength, (d) FWHM, and (e) γ of AuNPs synthesized in AC-PEG sol at different initial pH.

hydrogel formulation, also influencing the hydrogel's physicochemical and morphological properties.[52] Slightly alkaline pH was found to play a key role in the synthesis of AuNPs using PEG-driven reduction at high temperatures in water. Thanks to the excess hydroxyl groups, the equilibrium reported in eq 2 shifted toward the production of $AuCl_{x-n}(OH)_n$ oxides, species more prone to reduction compared to tetrachloroauric ions.[51]

$$AuCl_4^- + n{\cdot}OH^- \rightarrow AuCl_{4-n}(OH)_x + n{\cdot}Cl^- \quad (2)$$

NaOH has been used to provide OH^- to the reaction mixture, both in terms of pH change and in terms of the kinetic modification of AuNPs synthesis. To investigate its role in the reaction, two addition methods have been compared, following the proposed strategy. A schematic representation of the synthetic process has been proposed in Figure 1, reporting the methods described in our study.

3.1. One-Pot AuNPs Synthesis in AC-PEG Solution

One-pot synthesis and stabilization of AuNPs was adapted starting from a previously reported procedure in water.[57]

Briefly, the pH of the AC-PEG sol was adjusted by NaOH addition, and the system was preheated at 50 °C. An aliquot of $HAuCl_4$ solution was introduced into the reactive mixture, followed by microwave heating for 3 min at 80 °C. During this process, schematized in Figure 1a, the solution turned from transparent to purple, the typical color of colloidal AuNPs. Control reactions were initially carried out in solutions containing only carbomer (AC sol) or only PEG (PEG_{2000} sol) to elucidate the role of the individual components. AuNPs formation in AC sol exclusively occurred under strongly alkaline pH (∼11). Under these conditions, the reduction was most likely driven by NaOH, in a concentration-dependent manner,[58−61] while carbomer primarily acted as nanocrystals stabilizer via −COOH dissociation. Nevertheless, the reaction exhibited slow kinetics and a poor reaction yield (as reported in Figure S4a, Supporting Information). Conversely, AuNPs were effectively synthesized in PEG_{2000} sol; however, PEG_{2000} provided just mild stabilization in PBS, leading to rapid aggregation of the formed crystals (Figure S5, Supporting Information). Effective AuNPs synthesis and stabilization were achieved only in AC-PEG sol under the selected reactive conditions, yielding improved reaction kinetics and efficiency (Figure S4b, Supporting Information). Two key parameters have been systematically investigated to elucidate their influence on AuNPs synthesis: pH and $HAuCl_4$ concentration.

3.1.1. Effect of pH. The pH of the AC-PEG sol was adjusted within the range 6−11, excluding the intermediate pH

https://doi.org/10.1021/acsanm.5c05814
ACS Appl. Nano Mater. 2026, 9, 5067−5083

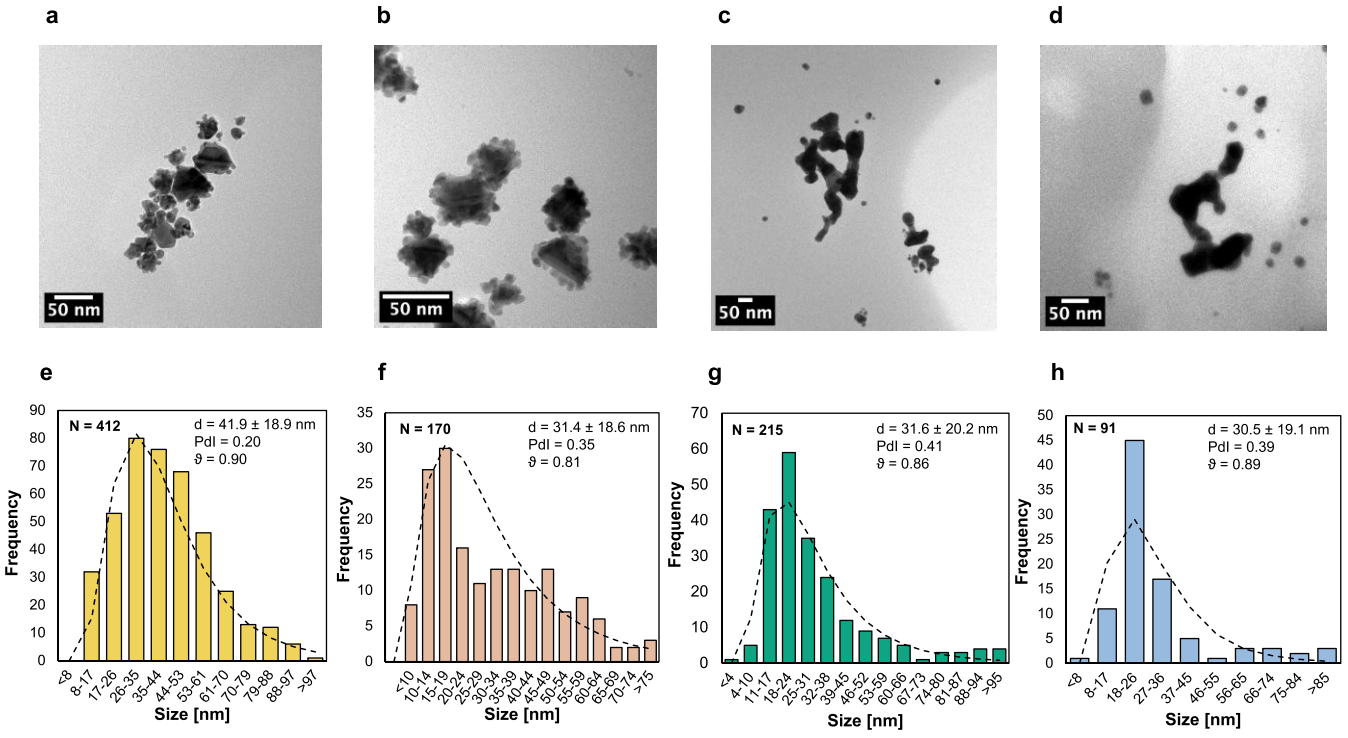

Figure 3. (a) TEM acquisition of AuNPs synthesized in AC-PEG sol at PEG/$HAuCl_4$ = 60 with initial pH 6, (b) pH 6.5, (c) pH 7, (d) pH 7.4. (e) Statistical size evaluation of AuNPs synthesized in AC-PEG sol at PEG/$HAuCl_4$ = 60 with initial pH 6, (f) pH 6.5, (g) pH 7, and (h) pH 7.4.

region (8−9), due to proximity to the solution equivalent point (Figure S6, Supporting Information). Lower pH values were not considered, as the resulting conditions were excessively acidic for AuNPs synthesis. Moreover, pH adjustment via HCl induced PEG precipitation in the solution. To isolate the pH effect, the reagent ratio was maintained constant at PEG/$HAuCl_4$ = 60.

Figure 2a,b reports the UV−vis spectra of the synthesized AuNPs as a function of the initial solution pH. The LSPR peak wavelength reached a minimum at pH 7.4, as shown in Figure 2c, indicative of a smaller AuNPs size. In contrast, both the full width at half-maximum (FWHM) and γ parameter (used to evaluate the optical features, and described in Figure S7, Supporting Information) reached the smallest values at pH 6.5. Notably, the optical polydispersity did not follow a consistent trend with the UV−vis-derived parameters, as reported in Figure 2d,e, suggesting a more complex dependence of the reaction conditions on the optical behavior.

Strongly alkaline conditions (pH 10 and pH 11) have been excluded from further analysis due to the broadened UV−vis spectra, large FWHM and γ, indicating poor spectral definition, and limited relevance to the intended purpose. TEM analysis was conducted to assess AuNPs morphology, size, and polydispersity. Across all the investigated pH, the synthesis predominantly yielded nonspherical AuNPs. Large quasi-spherical AuNPs were observed at mildly acidic pH (Figure 3a,b), whereas under neutral pH values (Figure 3c,d), the Au nanocrystals displayed asymmetrical growth with no evident control over spherical morphology. The largest AuNPs size was recorded at pH 6 (41.8 ± 18.9 nm) accompanied by a relatively high polydispersity index (PdI = 0.2), and a circularity parameter (ϑ) strongly deviating from unity.

Only in the case of pH 6 and 6.5, a few spherical-shaped NPs were observed in proximity to the bigger crystal surfaces, probably due to the interplay between nucleation and growth phenomena. UV−vis data reflect the global optical response of the dispersed nanoparticles. Consequently, the observation of aggregates with TEM does not necessarily contradict the presence of LSPR characteristics of dispersed particles, particularly in systems in which dispersed and aggregated nanoparticles coexist. In such cases, aggregation may predominantly be observed as broadening or tail contributions rather than a complete shift of the main LSPR peak.

The polymeric layer (PEG and carbomer) likely limited Au atom deposition, slowing particle growth and inducing the formation of smaller AuNPs adjacent to larger ones at the given pH. Conversely, nucleation was likely slower than growth at neutral pH, favoring the formation of amorphous-shaped AuNPs, as observed in Figure 3c,d. Although the reducing agent was present in large excess (PEG/$HAuCl_4$ = 60), its mild reducing capability extended the nucleation period and promoted the formation of larger AuNPs, particularly at neutral pH. The size distributions, reported in Figure 3e−3h, showed large AuNPs sizes and relatively large standard deviations (ranging from 41.8 ± 18.9 to 30.1 ± 19.1 nm), high PdI (ranging from 0.41 to 0.2), and circularities deviating from unity (from 0.81 to 0.9), in all analyzed cases. From an optical standpoint, the relatively elevated PdI values are expected to produce plasmon band broadening due to convolution of multiple LSPR contributions. This behavior is consistent with the observed FWHM and γ under the current reactive conditions. While moderate polydispersity does not inherently preclude biomedical applicability, excessively broad PdI may affect optical performance and sensing and photothermal applications. For this reason, further reaction conditions were explored to obtain improved AuNPs uniformity.

https://doi.org/10.1021/acsanm.5c05814
ACS Appl. Nano Mater. 2026, 9, 5067−5083

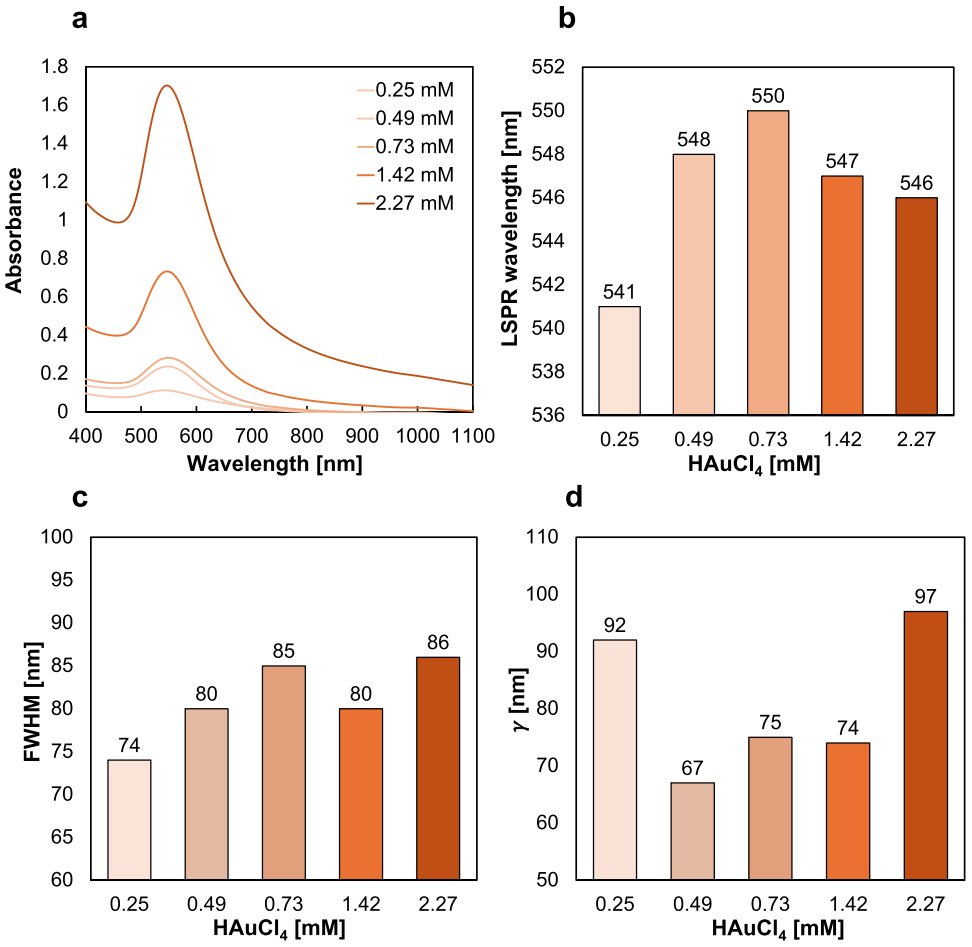

Figure 4. (a) UV−vis spectra of AuNPs synthesized in AC-PEG sol at initial pH 6.5 with different [$HAuCl_4$], corresponding to 12 ≤ PEG/$HAuCl_4$ ≤ 120; (b) LSPR peak wavelength, (c) FWHM, and (d) γ of AuNPs synthesized in AC-PEG sol at initial pH 6.5 with different [$HAuCl_4$].

3.1.2. Effect of $HAuCl_4$ Concentration. The effect of the $HAuCl_4$ concentration was investigated by fixing the initial pH at 6.5, a condition that previously produced a limited population of small spherical AuNPs. Progressive increases in the absorbance and LSPR shifts were observed by increasing the $HAuCl_4$ concentration, as evidenced from the UV−vis spectra reported in Figure 4a,b. Across all the stoichiometrically evaluated conditions, PEG was present in excess (12 ≤ PEG/$HAuCl_4$ ≤ 120), ensuring a suitable background for the $HAuCl_4$ reduction. The maximum LSPR peak wavelength was recorded at an $HAuCl_4$ concentration of 0.73 mM. The FHWM exhibited a consistent trend with the LSPR peak wavelength, whereas the γ parameter reached comparatively lower values within the Au precursor concentrations range 0.49−1.42 mM, as reported in Figure 4c,d. Notably, the overall optical properties did not follow a strictly predictable behavior, likely reflecting the residual sample inhomogeneity.

TEM analysis revealed a progressive improvement in the AuNPs morphological uniformity with increasing $HAuCl_4$ concentration. At $HAuCl_4$ concentrations of 1.42 and 2.27 mM (respectively in Figure 5b,c) predominantly spherical AuNPs were observed compared to the 0.49 mM case, shown in Figure 5a,d. The most favorable size distribution was observed at 1.42 mM (Figure 5e), yielding AuNPs with a mean diameter of 25.4 ± 12.5 nm (PdI = 0.24, ϑ = 0.91). On the other hand, the highest circularity ϑ and lowest PdI values were recorded at 2.27 mM, corresponding to slightly larger AuNPs (diameter = 32.2 ± 12.7 nm, PdI = 0.15, ϑ = 0.93), as reported in Figure 5f. The observed trend suggests that by decreasing the PEG excess, the nucleation process was kinetically favored over the growth on previously formed crystals.

3.2. One-Pot AuNPs Synthesis in AC-PEG Solution with NaOH Postsynthesis Addition

To elucidate the role of NaOH in the synthesis, an alternative experimental strategy was adopted, in which NaOH was introduced at different stages of the reaction. The NaOH addition, either prior to or following microwave irradiation, influenced the UV−vis spectra, affecting the LSPR peak intensity, wavelength, and FWHM (as shown in Figure S8a, Supporting Information). Postsynthetic NaOH addition produced a blue-shifted and sharper LSPR band, while the solution exhibited a more rapid color intensification compared to NaOH addition before the reaction, suggesting a NaOH-mediated enhancement of the AuNPs nucleation process.

The influence of NaOH addition timing on AuNPs properties was further assessed (Figure S8b, Supporting Information), identifying optimal conditions when NaOH was added after 60 s of microwave treatment (equivalent to T = 70 °C), as reported in the schematic representation in Figure 1b. Consistently, the spectral features indicated a clear dependence of AuNPs optical properties on NaOH concentration. Therefore, the influence of both the NaOH amount

https://doi.org/10.1021/acsanm.5c05814
ACS Appl. Nano Mater. 2026, 9, 5067−5083

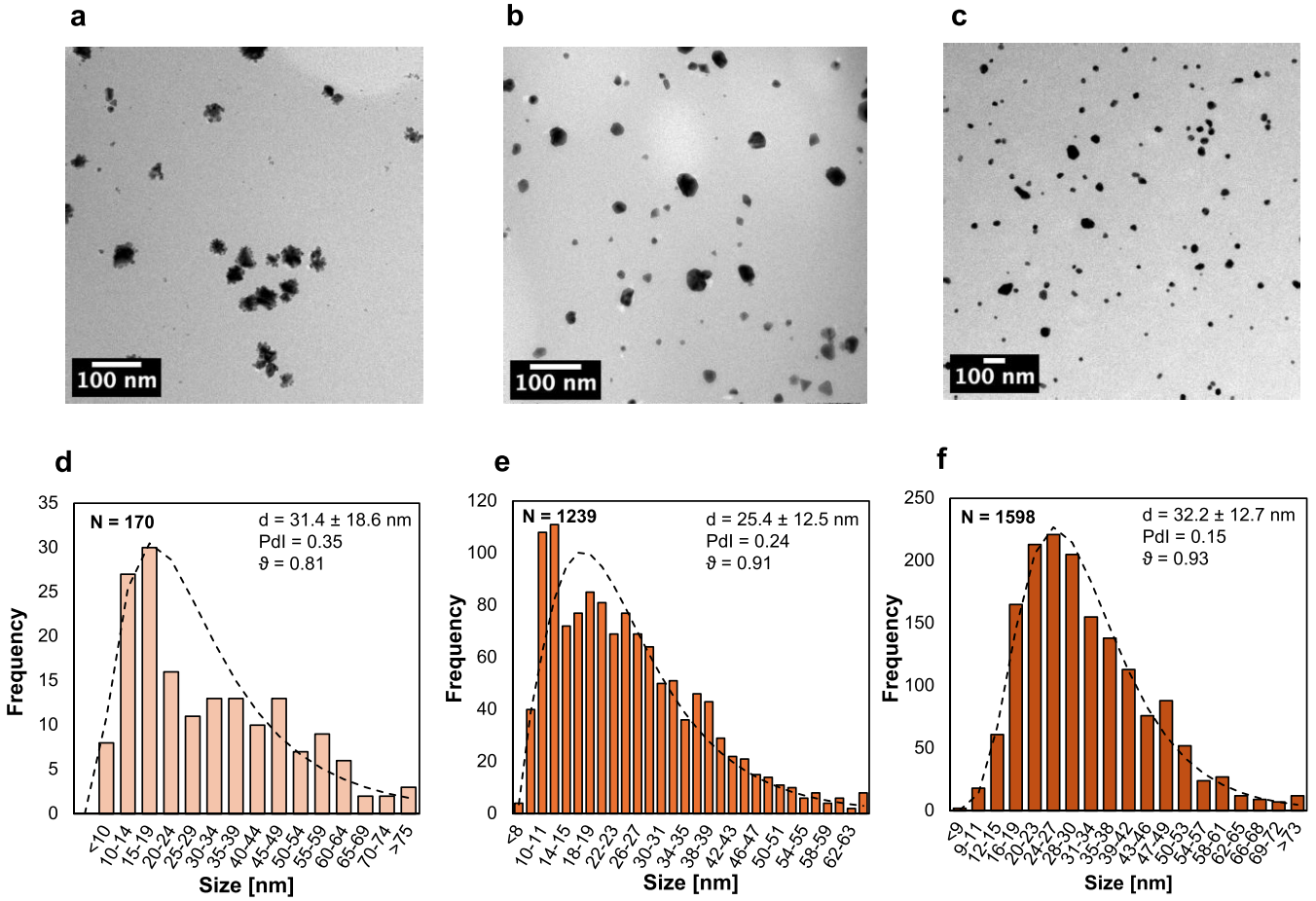

Figure 5. (a) TEM acquisition of AuNPs synthesized in AC-PEG sol at initial pH 6.5 with $[HAuCl_4]$ = 0.49 mM, (b) $[HAuCl_4]$ = 1.42 mM, and (c) $[HAuCl_4]$ = 2.27 mM. (d) Statistical size evaluation of AuNPs synthesized in AC-PEG sol at initial pH 6.5 with $[HAuCl_4]$ = 0.49 mM, (e) $[HAuCl_4]$ = 1.42 mM, and (f) $[HAuCl_4]$ = 2.27 mM.

and the $HAuCl_4$ concentration was systematically investigated within this synthetic framework.

3.2.1. Effect of NaOH Addition Concentration. The synthesis has been performed at an initial AC-PEG sol pH of 6.5 and a fixed PEG/$HAuCl_4$ = 60, employing different NaOH/$HaAuCl_4$ ratios (hereafter denoted as Φ, for simplicity), to determine the influence of NaOH addition on AuNPs properties. Φ was varied within a defined interval to achieve a final solution pH in the range 6.1−7.4.

The UV−vis spectra of the synthesized AuNPs are presented in Figure 6a. The spectra revealed a progressive absorbance increase with increasing NaOH addition up to Φ = 36.8. The LSPR peak wavelengths showed the minimum values within the interval $25.7 \leq \Phi \leq 33.1$ (Figure 6b). A comparable trend was observed for both the FWHM and γ, demonstrating the narrowest LSPR band profiles at Φ = 29.4 and 33.1, as displayed in Figure 6c,d.

TEM analysis corroborated the UV−vis spectra observations. In Figure 7a, AuNPs synthesized with Φ = 14.7 appeared inhomogeneous, with pronounced aggregation in irregular morphologies. By contrast, Φ = 33.1, as reported in Figure 7b, yielded smaller and morphologically uniform AuNPs. Further increasing the Φ to 44.1, as shown in Figure 7c, again resulted in heterogeneous and irregularly shaped Au nanocrystals.

The most favorable synthetic conditions were identified at Φ = 33.1, yielding AuNPs with a mean diameter of 16.2 ± 7.1 nm (PdI = 0.19, ϑ = 0.93), as displayed in Figure 7e.

These features represent a clear improvement compared to both Φ = 14.7 (diameter size = 34.5 ± 19.9 nm, PdI = 0.33, ϑ = 0.87) and Φ = 44.1 (diameter size = 31.2 ± 17.9 nm, PdI = 0.14, ϑ = 0.75), respectively, reported in Figure 7d,f. Overall, the size distributions, morphological sphericity, and PdI values were markedly improved, relative to the one-pot synthesis performed without NaOH addition. These findings highlight the role of postsynthetic NaOH introduction in promoting the formation of smaller and more uniformly distributed AuNPs, consistent with a nucleation-favored growth regime (as summarized in Figure S9, Supporting Information). The synthetic conditions involving NaOH addition were further summarized in a two-dimensional representation in Figure S10 (Supporting Information), correlating the full UV−vis spectra with both the Φ ratio and the normalized absorbance/γ. The latter metric quantifies the trade-off between a high AuNPs concentration (given by high absorbance) while maintaining a low PdI (indicated by low γ). Accordingly, the optimal synthetic conditions were identified within the interval $30 \leq \Phi \leq 35$, corresponding to NaOH concentration of approximately 14−15 mM. Under these conditions, a narrow UV−vis spectra peak, resonant wavelength between 520 and 530 nm, and a high absorbance/γ ratio were observed.

3.2.2. Effect of $HAuCl_4$ Concentration with NaOH Addition. The effect of $HAuCl_4$ concentrations on the final AuNPs properties was studied under NaOH postsynthetic addition, maintaining an initial AC-PEG sol pH of 6.5. The

https://doi.org/10.1021/acsanm.5c05814
ACS Appl. Nano Mater. 2026, 9, 5067−5083

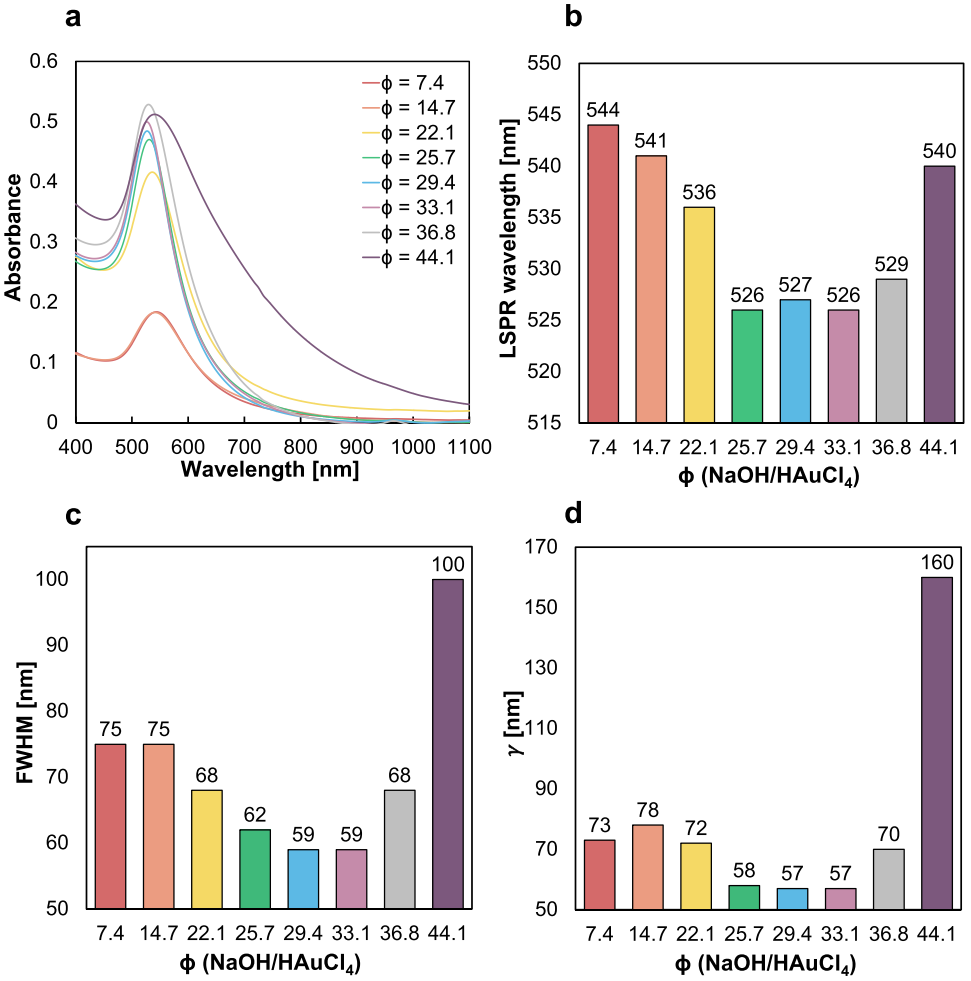

Figure 6. (a) UV−vis spectra of AuNPs synthesized in AC-PEG sol at initial pH 6.5 and PEG/$HAuCl_4$ = 60, with NaOH postsynthetic addition at ratio Φ (NaOH/$HAuCl_4$) in the range 7.4−44.1. (b) LSPR peak wavelength, (c) FWHM, and (d) γ of AuNPs synthesized in AC-PEG sol at initial pH 6.5 and PEG/$HAuCl_4$ = 60 at different Φ.

NaOH concentration was fixed at 14.2 mM in the final solution, corresponding to a final pH around 7−7.4. The UV−vis spectra of the synthesized AuNPs are reported in Figure 8a. The increase in $HAuCl_4$ produced a gradual enhancement of the LSPR peak intensity, exhibiting a linear dependence within the $HAuCl_4$ concentration range 0.25−0.73 mM (Figure S11a, Supporting Information). The LSPR peak wavelength showed a minimum at 1.42 mM, as shown in Figure 8b.

The FWHM followed a trend consistent with the LSPR peak wavelength, also reaching a minimum at 1.42 mM $HAuCl_4$, whereas the γ parameter remained comparatively stable when $HAuCl_4$ concentration was in the range 0.49−1.42 mM, as respectively shown in Figure 8c,d. Also in this case, the UV−vis spectra generally showed narrower curve shapes and a better linear increase compared with the one-pot synthesis performed without NaOH addition, further indicating improved optical properties of the resulting AuNPs.

TEM analysis confirmed that AuNPs showed predominantly spherical shapes across all of the investigated $HAuCl_4$ concentrations, as represented in Figure 8e−8h. As expected from the UV−vis data, AuNPs showed a reduced mean diameter compared to the one-pot synthetic method, in agreement with the blue-shifted plasmonic peaks. The size distributions were centered at smaller values, with mean particle size ranging from 14.1 ± 4.6 nm to 18.4 ± 5.4 nm. Improved PdI values were obtained in all cases (0.08−0.11), and circularities approaching unity (ϑ = 0.89−0.92) as summarized in Figure 8i−8l. The best conditions were recorded at a $HAuCl_4$ concentration of 1.42 mM, which yielded AuNPs with a mean size of 14.1 ± 4.6 nm (PdI = 0.1, ϑ = 0.92) corresponding to the AuNPs population reported in Figure 8g,k.

3.2.3. One-Pot vs NaOH Postsynthesis Addition Method. Overall, considering all the variables collectively, the postsynthetic NaOH addition strategy provided several advantages compared to the simple one-pot synthesis performed in AC-PEG sol. As already described, the method enabled a better control on AuNPs morphology, size distribution, and optical properties. The yielded AuNPs were characterized by low PdI values and circularity close to unity, representing an advantage for applications in which uniform size and optical properties are crucial, e.g., sensing. Additionally, starting from a mildly acidic AC-PEG sol (pH = 6.5), near-neutral conditions were achieved through NaOH addition under the optimized parameters, representing an ideal scenario for the *in situ* AuNPs synthesis within the hydrogel.

In contrast, the one-pot method remained effective in reducing $HAuCl_4$, despite the nonoptimized conditions resulting in less uniform AuNPs populations and broader size distributions. The main outcomes for the two synthetic

https://doi.org/10.1021/acsanm.5c05814
ACS Appl. Nano Mater. 2026, 9, 5067−5083

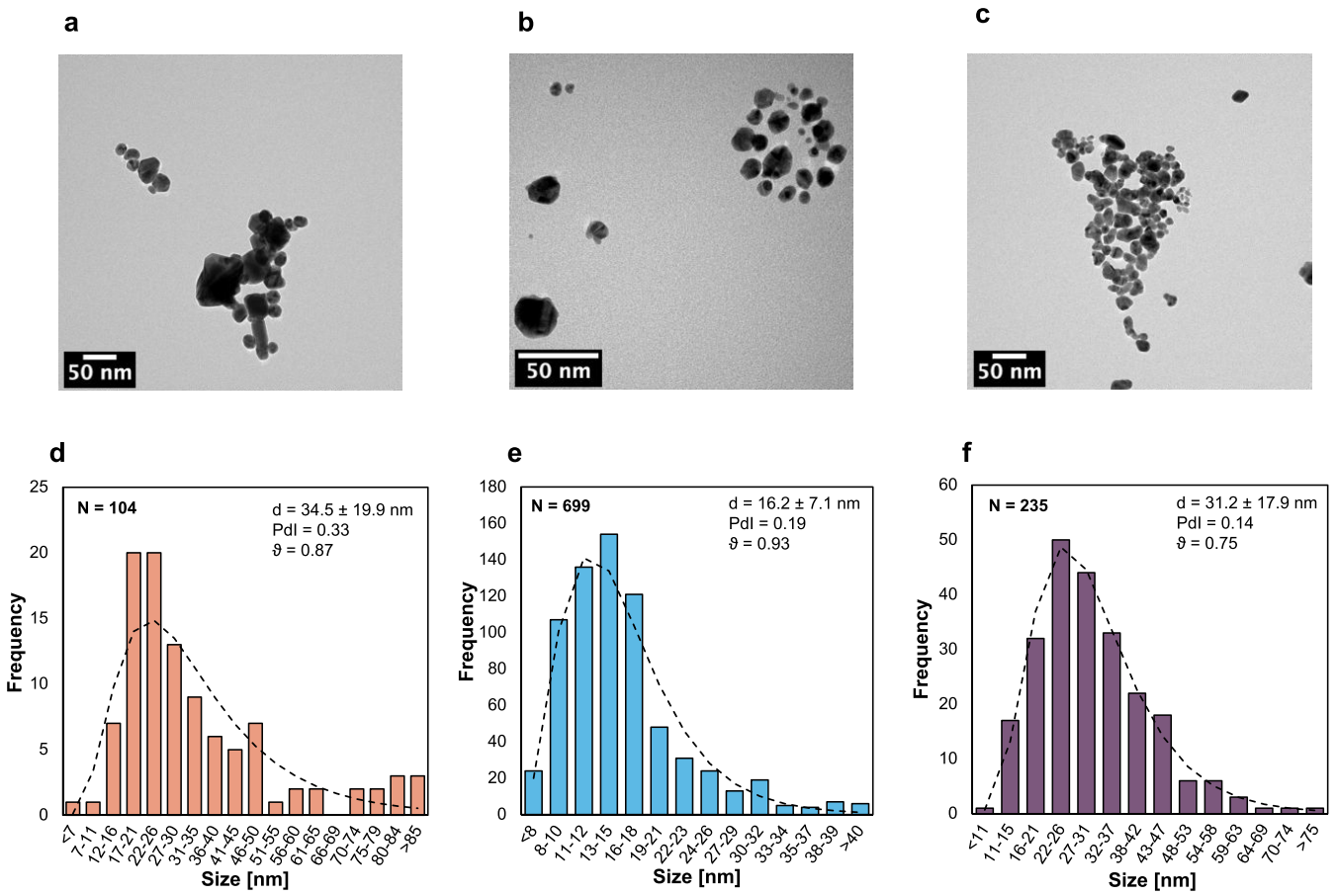

Figure 7. (a) TEM acquisition of AuNPs synthesized in AC-PEG sol at initial pH 6.5 and PEG/$HAuCl_4$ = 60, with NaOH postsynthetic addition at ratio Φ = 14.7, (b) Φ = 29.4, (c) Φ = 44.1. (d) Statistical size evaluation of AuNPs synthesized in AC-PEG sol at initial pH 6.5 and PEG/$HAuCl_4$ = 60, with NaOH postsynthetic addition at ratio Φ = 14.7, (e) Φ = 29.4, (f) Φ = 44.1.

routes are summarized in Tables S1 and S2. ICP-EOS spectroscopy was employed to quantify AuNPs concentration under postsynthetic NaOH addition, resulting in Au content in the range between 6.1 and 57.3 mg/L across the investigated precursor concentrations ([$HAuCl_4$] = 0.25−2.27 mM). The reaction yield was around 70−75% as reported in Table S3 (Supporting Information), likely reflecting the mild reducing capability of PEG. The final AuNPs densities were in the range 3.8×10^{11}−1.7×10^{12} NPs/mL. A consistent qualitative agreement was observed between AuNPs concentration and UV−vis optical properties. Higher ICP-measured Au content displayed an increased UV−vis absorbance intensity, supporting the expected concentration-dependent optical behavior. The observed trend followed a logarithmic trend (Figure S11b, Supporting Information). Deviations from strict linear proportionality (Lambert−Beer behavior) in plasmonic nanoparticles might be attributed to variations in the reaction yield, AuNPs size distribution, and plasmon band broadening, as reflected by the FWHM and γ parameters. Additionally, phenomena such as multiple scattering and size-dependent extinction cross sections become significant with nanoparticles concentration. Under such conditions, the optical response reflects collective electromagnetic effects rather than a concentration-dependent process, which is out of the scope of our discussion.

3.3. *In Situ* AuNPs Synthesis in AC-PEG Hydrogel

The synthetic method previously optimized in AC-PEG sol was modified by agarose incorporation to enable the synthesis of AuNPs together with the formation of the hydrogel matrix, as schematized in Figure 1c. The AC-PEG hydrogel formulation was obtained through a microwave-assisted polycondensation reaction involving the −OH groups in agarose and the −COOH groups of carbomer.

Microwave irradiation enables the rapid, homogeneous, and volumetric heating of the reactive medium. Additionally, in view of the scalable application of the method, microwave reactors provide control over the evaporation rate of the aqueous phase. This latter aspect is particularly critical for hydrogel-based systems, where variations in the component concentration may affect the final properties. PEG and glycerol functioned as additional cross-linkers, contributing to enhance the network density. A schematic representation of the chemical reaction is presented in Figure 9a. The formulation has been selected based on the dual role of PEG, acting both as a reducing agent for $HAuCl_4$ and cross-linker for the hydrogel matrix. Moreover, its biocompatibility has been previously validated in both *in vitro* and *in vivo* models.[62,63] For hydrogel preparation, the AC-PEG solution pH was adjusted to 6.5, and the addition of NaOH was fixed to have a final concentration of 14.2 mM, whereas the $HAuCl_4$ concentration was varied within the previously established range. FT-IR spectra of blank AC-PEG and AuNPs/AC-PEG, reported in Figure 9b, did not

https://doi.org/10.1021/acsanm.5c05814
ACS Appl. Nano Mater. 2026, 9, 5067−5083

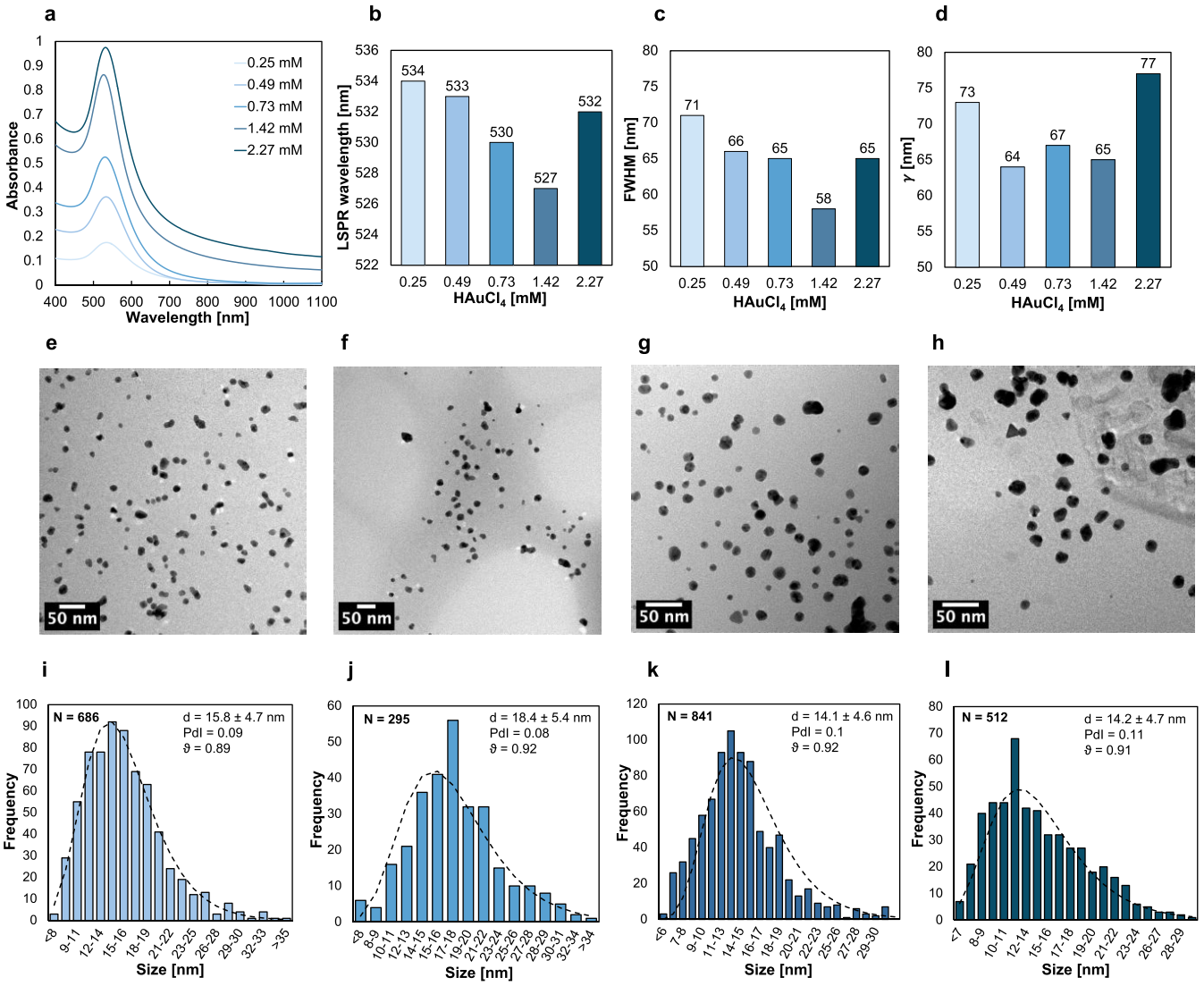

Figure 8. (a) UV−vis spectra of AuNPs synthesized in AC-PEG sol at initial pH 6.5 with NaOH postsynthetic addition at [NaOH] = 14.2, with different [$HAuCl_4$] corresponding to 12 ≤ PEG/$HAuCl_4$ ≤ 120. (b) LSPR wavelength, (c) FWHM, and (d) γ of AuNPs synthesized in AC-PEG sol at initial pH 6.5, with NaOH postsynthetic addition at [NaOH] = 13 and different [$HAuCl_4$]. (e) TEM acquisition of AuNPs synthesized in AC-PEG sol at initial pH 6.5 with postsynthetic addition at [NaOH] = 13, at [$HAuCl_4$] = 0.49 mM, (f) [$HAuCl_4$] = 0.73 mM, (g) [$HAuCl_4$] = 1.42 mM, (h) [$HAuCl_4$] = 2.27 mM. (i) Statistical size evaluation of AuNPs synthesized in AC-PEG sol at initial pH 6.5 with NaOH postsynthetic addition at [NaOH] = 13, at [$HAuCl_4$] = 0.49, (j) [$HAuCl_4$] = 0.73 mM, (k) [$HAuCl_4$] = 1.42 mM, (l) [$HAuCl_4$] = 2.27 mM.

reveal significant spectral differences, demonstrating that AuNPs *in situ* synthesis did not compromise the hydrogel network formation. Specifically, the broad peak between 3600 and 3100 cm^{-1} represents the −OH bonds stretching and vibration, particularly referring to free −OH and inter- and intramolecular H bonds. The region between 3000 and 2750 cm^{-1} corresponds to the stretching of C−H bonds in the aliphatic polymer backbone. The peak at 1650 cm^{-1} is representative of C═O stretching in the ester bonds, confirming the polycondensation reaction formation, while the peak at 1560 cm^{-1} corresponds to the C═O stretching of carboxylates, together with the 1420 cm^{-1} one. The peaks in the region 1440−1390 cm^{-1} and 1300−1120 cm^{-1} are, respectively, associated with C−O−H bending on the plane and C−O stretching. Lastly, the wide region 1400−900 cm^{-1} is associated with the bending of the alcohols −OH (1410−1230 cm^{-1}), stretching of the C−O group in ethers (1400−1200 cm^{-1}), and the stretching of alcohols C−O groups (1200−900 cm^{-1}). The DCS analysis (Figure S12a, Supporting Information) further confirmed that AuNPs synthesis did not affect the material's thermal behavior.

The melting and crystallization enthalpies of the samples differed by less than 5 J/g, with the values, respectively, around H_m = 98.35 J/g and H_c = −88.991 J/g. From visual inspection, the hydrogel after prolonged soaking in PBS (4 weeks, Figure S12b, Supporting Information) revealed a homogeneous appearance without evidence of macroscopic AuNPs precipitation. Although nanoscale rearrangements cannot be excluded based on visual assessment, no macroscopic instability was observed.

3.3.1. Swelling Characterization. The swelling behavior of the nanocomposite hydrogel was evaluated as a function of the AuNP concentration within the polymeric network. Swelling kinetics were not significantly influenced by the AuNPs concentration within the hydrogel, as reported in detail in Figure S13 (Supporting Information). Across all the

https://doi.org/10.1021/acsanm.5c05814
ACS Appl. Nano Mater. 2026, 9, 5067−5083

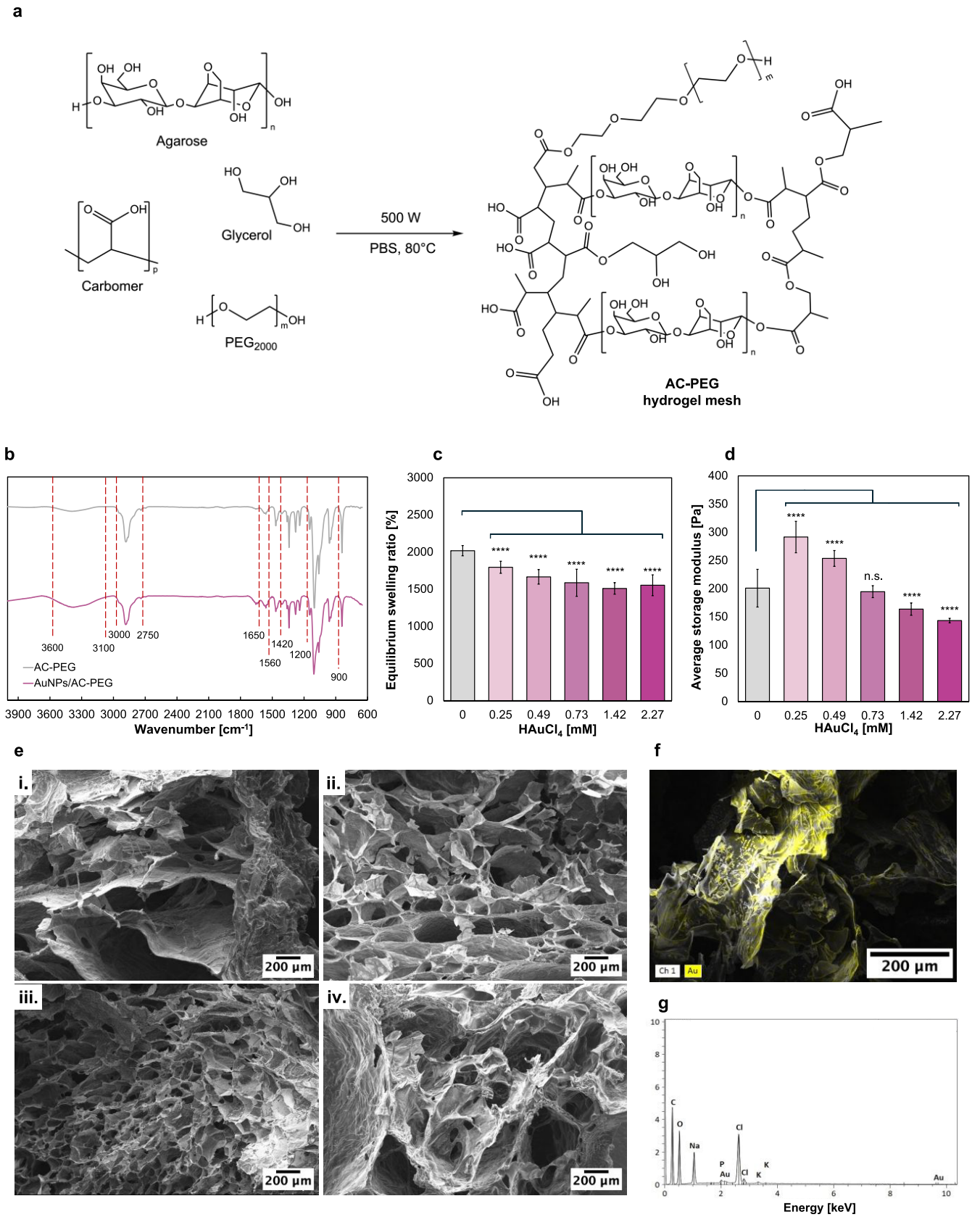

Figure 9. (a) Chemical reaction of hydrogel formation showing the chemical structure of the AC-PEG network. (b) FT-IR spectra of AC-PEG (gray) and AuNPs/AC-PEG (purple). (c) Equilibrium swelling ratio comparison between AC-PEG hydrogel (blank) and AuNPs/AC-PEG hydrogel synthesized at different AuNPs concentrations (using $HAuCl_4$ concentrations in the range 0.25−2.27 mM). Results reported as mean ± standard deviation ($N = 4$, ****, $p < 0.0001$). (d) Comparison of average G' values evaluated within the LVE region of AC-PEG and AuNPs/AC-PEG at different AuNPs concentrations. Results reported as mean ± standard deviation ($N = 4$, n.s., $p > 0.05$; ****, $p < 0.0001$). (e) SEM acquisitions of (i) AC-PEG, (ii) AuNPs/AC-PEG synthesized at 0.25 mM $HAuCl_4$, (iii) AuNPs/AC-PEG synthesized at 0.73 mM $HAuCl_4$, (iv)

https://doi.org/10.1021/acsanm.5c05814
ACS Appl. Nano Mater. 2026, 9, 5067−5083

Figure 9. continued

AuNPs/AC-PEG synthesized at 2.27 mM $HAuCl_4$. (f) SEM coupled EDX acquisition of AuNPs/AC-PEG synthesized at 2.27 mM $HAuCl_4$ and (g) EDX elemental map where Au presence peaks underline the presence of AuNPs.

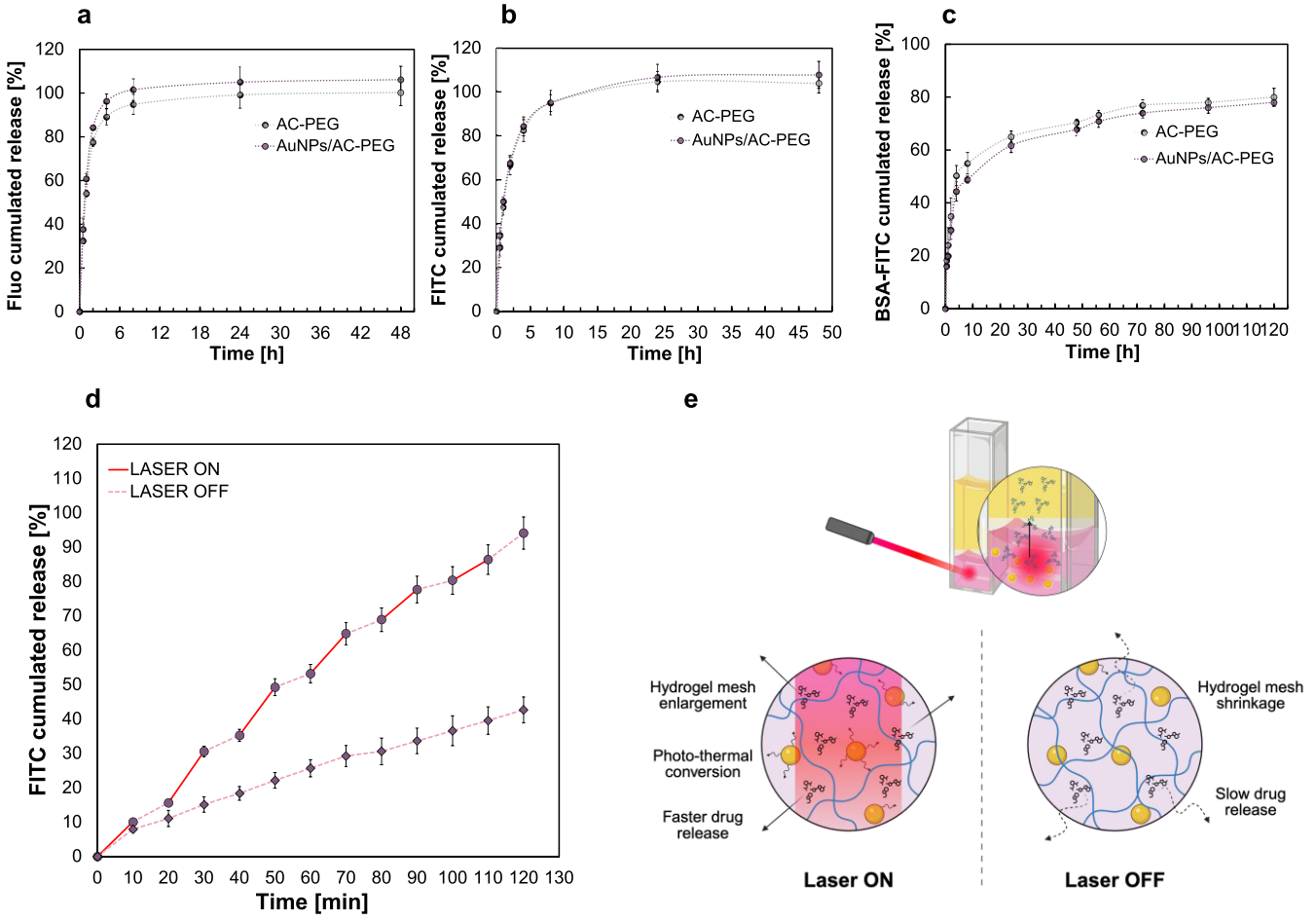

Figure 10. (a) Cumulated release profile of Fluo, (b) FITC, and (c) BSA-FITC from AC-PEG (gray) and AuNPs/AC-PEG (purple), synthesized at 2.27 mM $HAuCl_4$. (d) Comparison of the cumulated FITC release profile from AuNPs/AC-PEG synthesized at 2.27 mM $HAuCl_4$ without laser irradiation (dashed line) and under 10 min ON-OFF laser irradiation cycles (ON: full line, OFF: dashed line). (e) Schematic representation of the irradiation process and the involved phenomena. Results are presented as mean ± standard deviation, and the obtained values were evaluated with measurements run at least in triplicate.

investigated $HAuCl_4$ concentrations, the swelling profiles reached a plateau corresponding to the equilibrium swelling state within approximately 1−1.5 h, indicating that the variation in AuNPs content does not affect the hydrogel rehydration rate. Conversely, the equilibrium swelling ratio (Figure 9c) exhibited an AuNPs concentration-dependent decrease for AuNPs/AC-PEG relative to the pristine hydrogel, with values ranging between 2000 and 1500%. This behavior may be attributed to the AuNPs' presence, acting as filler and spacer inside the hydrogel, thus limiting the amount of reabsorbed water from the hydrogel mesh. Additionally, structural modifications associated with the reduction of $HAuCl_4$ cannot be excluded. The partial oxidation of PEG hydroxyl groups, together with AuNPs surface stabilization mediated by PEG and carbomer, may result in variation of cross-linking densities. Such effects could influence the swelling behavior of the nanocomposite system. Moreover, hydrogels exhibit swelling behavior governed by counterion osmotic pressure. Partial involvement of carbomer functionalities in AuNP stabilization may reduce the concentration of osmotically active counterions, contributing to the observed decrease in equilibrium swelling.

3.3.2. Rheological Characterization. The rheological properties of the nanocomposite hydrogel have been evaluated as a function of the AuNPs concentration. Amplitude sweep tests demonstrated a solid-like behavior of the AuNPs/AC-PEG hydrogel across the investigated $HAuCl_4$ concentrations, with $G' \gg G''$ within the limit of the linear viscoelastic (LVE) region, observed around 1% strain for all the samples (Figure S14a, Supporting Information). The average G' values measured within the LVE region (Figure 9d) exhibited increased values at low Au precursor concentrations (0.25 and 0.49 mM) compared to the blank AC-PEG samples (respectively, 292 and 254 Pa vs 201 Pa), suggesting a reinforcing contribution from AuNPs. Conversely, at higher $HAuCl_4$ concentration, a gradual reduction of the average G' was observed. This behavior likely reflects nanoparticle-induced local alteration of the network structure. Increased

https://doi.org/10.1021/acsanm.5c05814
ACS Appl. Nano Mater. 2026, 9, 5067−5083

AuNPs content may introduce steric constraints and local rigidity, limiting polymer chain interactions, mobility, and elastic response. In addition, beyond steric effects, in situ AuNPs formation may influence the network by affecting the availability of the polymers' functional groups involved in the cross-linking. the cross-linking. Indeed, interactions involving the carbomer and PEG during nanoparticle reduction and stabilization could modify the extent of ester bond formation during the polycondensation reaction. This could potentially lead to network reorganization, contributing to the observed modulus reduction.

Consistent with these interpretations, the average storage moduli of AuNPs/AC-PEG at $HAuCl_4$ concentrations higher than 0.73 mM were lower than G' recorded for the blank AC-PEG hydrogel. Overall, the mechanical response of the system appears to be governed by a balance between nanoparticle reinforcement and hydrogel network perturbation effects. Frequency sweep test further demonstrated a solid-like behavior of pristine AC-PEG hydrogel, in a frequency range from 0.1 to 100 rad/s (as shown in Figure S14b, Supporting Information).

3.3.3. SEM Characterization. SEM analysis was performed to investigate the morphological features of the nanocomposite hydrogels. No significant differences were observed between AuNPs/AC-PEG and AC-PEG samples (at different AuNPs concentrations, i.e., 0.25 mM $HAuCl_4$, 0.49 mM $HAuCl_4$, and 2.27 mM $HAuCl_4$), as shown in Figure 9e. All hydrogels displayed interconnected porosity with a honeycomb-like porous structure and heterogeneous pore size distribution. Energy dispersive X-ray (EDX) spectroscopy confirmed the presence of AuNPs within the polymeric matrix, as evidenced by both the elemental mapping (Figure 9f) and the characteristic Au signal in the corresponding spectrum (Figure 9g).

3.3.4. Mimetic-Drug Delivery Characterization. Drug release experiments were performed using three model drug mimetics loaded into AuNPs/AC-PEG (formulated at a fixed $HAuCl_4$ concentration of 2.27 mM) and pristine AC-PEG hydrogels. Fluorescein (Fluo), FITC, and BSA-FITC have been selected as representative drug mimetics to capture broad physicochemical characteristics in terms of size and solubility, namely, small hydrophilic and hydrophobic molecules, and a hydrophilic sterically hindered high macromolecular species. Application-specific behavior and charge-mediated interactions with relevant therapeutic compounds remain subjects of future investigation.

The cumulated release profiles, shown in Figure 10, demonstrated minimal and statistically not significant differences between the pristine AC-PEG and AuNPs/AC-PEG hydrogel, indicating that the presence of *in situ*-synthesized AuNPs did not alter the drug delivery performance of the system. While both Fluo and FITC were completely released after approximately 24 h, Fluo exhibited slightly faster release kinetics (Figure 10a) compared to FITC (Figure 10b), likely due to their distinct physicochemical nature. Conversely, BSA-FITC release kinetics was consistently slower, characterized by an initial burst release during the first 8 h and a cumulative release of approximately ∼80% over 5 days, as reported in Figure 10c.

3.3.5. Laser-Assisted Mimetic-Drug Delivery. The cumulative drug release under laser irradiation was investigated in AuNPs/AC-PEG hydrogel to test whether the plasmonic properties of AuNPs could influence the release performance through laser-induced thermal enhancement. FITC-loaded AuNPs/AC-PEG hydrogels were formulated at 2.27 mM $HAuCl_4$ to maximally exploit AuNPs thermal conversion, which is known to depend on AuNPs concentration. AuNPs/AC-PEG hydrogels were subjected to ON-OFF irradiation cycles of 10 min. The cumulative FITC release, reported in Figure 10d, demonstrated a pronounced increment in the amount of FITC released under laser irradiation compared to the sample not subjected to laser irradiation over the 2 h experimental window. During irradiation periods, the release curves exhibited markedly steeper slopes, whereas upon cessation of laser exposure, the release rates returned to values comparable to the control samples. The laser wavelength employed (632 nm) does not spectrally overlap with the absorption band of FITC (peak at 495 nm). Significant direct bleaching is not expected under these conditions. Furthermore, dye release was quantified by UV−visible absorbance rather than fluorescence, minimizing potential bias from quenching effects. The cumulated release of the irradiated samples reached approximately 80%, corresponding to nearly a 2-fold increase relative to the control. This behavior is primarily attributed to localized light-induced heating in the presence of AuNPs, which may promote a transient polymeric matrix stretch and enhanced mimetic drug diffusional transport. Such effects were identified as the main factor responsible for the enhanced release kinetics and increased equilibrium values observed in laser-irradiated samples, as schematized in Figure 10e.

Due to the low irradiation power and the low heat conductivity of the aqueous hydrogel matrix, bulk temperature variations are expected to be minimal and difficult to resolve with conventional probes. Nevertheless, localized effects in the irradiated region may still contribute to the observed light-enhanced release. Conventional thermal probes may not provide robust or spatially resolved information, and advanced sensing methods, e.g., fiber Bragg grating sensors, would be required, as demonstrated in comparable hydrogel systems.[64] However, these quantifications are beyond the present scope while representing an important direction for future investigations.

4. CONCLUSIONS

In situ synthesis of AuNPs has emerged as an attractive strategy to simplify hydrogel nanocomposite fabrication by overcoming the challenges associated with nanoparticles incorporation. In this work, a one-pot microwave-assisted process enabled the simultaneous synthesis of AuNPs and the formation of a hydrogel matrix composed of agarose, carbomer, and PEG in PBS. The findings indicate that PEG acts as a reducing agent for the Au precursor, playing a critical role in stabilizing the nanoparticle system under physiologically relevant ionic condition, in combination with carbomer. Systematic variation of the synthetic parameters led to controlled AuNPs formation, while postsynthetic NaOH addition further improved the nanoparticles uniformity (size reduced by ∼10 nm, enhanced circularity, and polydispersity). The resulting AuNPs/AC-PEG nanocomposites preserved the internal morphology, while showing concentration-dependent swelling and rheological behavior. Laser-assisted release tests revealed light-modulated molecular delivery, consistent with AuNPs photothermal properties. Under the employed low laser power regime, localized thermal contributions are expected to influence the observed release behavior over macroscopic temperature

https://doi.org/10.1021/acsanm.5c05814
ACS Appl. Nano Mater. 2026, 9, 5067−5083

variations. Although the results highlight the potential of the proposed system, certain aspects merit further investigation.

In particular, high-resolution thermal mapping, AuNPs distribution within the hydrogel matrix, and systematic evaluation of the release of electrostatically charged and clinically relevant therapeutics would provide valuable insights. Overall, this approach provides a facile route for generating AuNP-loaded hydrogels, supporting their potential use as light-responsive systems for drug delivery and other biomedical applications.

■ ASSOCIATED CONTENT

Supporting Information

The Supporting Information is available free of charge at https://pubs.acs.org/doi/10.1021/acsanm.5c05814.

AuNPs synthetic procedure using the classic and the microwave-heating modified Turkevich method; drug mimetics absorbance calibration lines; UV−vis, TEM, and size distribution of AuNPs using the classic and microwave-heating Turkevich methods; scheme of $HAuCl_4$ reduction by PEG; UV−vis spectra comparison of AuNPs synthesized in AC sol and AC sol; UV−vis spectra of AuNPs synthesized in PEG2000 and picture; titration curves of AC sol and AC-PEG; graphical evaluation of the optical parameters from UV−vis spectra; comparison of pre- and postsynthetic addition of NaOH at different concentrations and time of addition; synthetic outcomes (UV−vis spectra, TEM images and size distribution) from the one-pot and one-pot with postsynthetic NaOH addition methods; controur map of the optimal synthetic conditions obtained from the experimental data; summary tables of the synthetic parameter and outcomes of the one-pot and one-pot with NaOH postsynthetic addition; experimental fitting of UV−vis absorbance vs $HAuCl_4$ or Au concentration; differential scanning calorimetry spectra of the hydrogels; image of AuNPs/AC-PEG hydrogel stability after 4 weeks soaking in PBS; swelling kinetics of the AuNPs/AC-PEG hydrogels; and rheological tests of AuNPs/AC-PEG and pristine hydrogels synthesized with different Au precursor concentrations (PDF)

■ AUTHOR INFORMATION

Corresponding Author

Filippo Rossi − *Dipartimento di Chimica, Materiali e Ingegneria Chimica "G. Natta", Politecnico di Milano, Milan 20131, Italy;* orcid.org/0000-0003-2665-120X; Email: filippo.rossi@polimi.it

Authors

Alessandro Molinelli − *Dipartimento di Chimica, Materiali e Ingegneria Chimica "G. Natta", Politecnico di Milano, Milan 20131, Italy;* orcid.org/0000-0001-9230-9360

Julián Guacaneme Sánchez − *Dipartimento di Chimica, Materiali e Ingegneria Chimica "G. Natta", Politecnico di Milano, Milan 20131, Italy;* orcid.org/0009-0000-7812-3754

Andrea Schirato − *Dipartimento di Fisica, Politecnico di Milano, Milan 20133, Italy; Department of Physics and Astronomy, Rice University, Houston, Texas 77005, United States;* orcid.org/0000-0001-8024-9778

Francesco Briatico Vangosa − *Dipartimento di Chimica, Materiali e Ingegneria Chimica "G. Natta", Politecnico di Milano, Milan 20131, Italy;* orcid.org/0000-0002-7088-1064

Margherita Maiuri − *Dipartimento di Fisica, Politecnico di Milano, Milan 20133, Italy;* orcid.org/0000-0001-9351-8551

Complete contact information is available at: https://pubs.acs.org/10.1021/acsanm.5c05814

Notes

The authors declare no competing financial interest.

■ REFERENCES

(1) Giljohann, D. A.; Seferos, D. S.; Daniel, W. L.; Massich, M. D.; Patel, P. C.; Mirkin, C. A. Gold Nanoparticles for Biology and Medicine. *Angew. Chem., Int. Ed.* **2010**, *49* (19), 3280−3294.

(2) Fernandez Alarcon, J.; Perez Schmidt, P.; Panini, N.; Caruso, F.; Violatto, M. B.; Sukubo, N. G.; Martinez-Serra, A.; Ekalle-Soppo, C. B.; Morelli, A.; Moscatiello, G. Y.; Grasselli, C.; Corbelli, A.; Fiordaliso, F.; Kelk, J.; Petrosilli, L.; d'Orazio, G.; Mateu Ferrando, R.; Verdaguer Ferrer, A.; Fornaguera, C.; Lay, L.; Fumagalli, S.; Recchia, S.; Monopoli, M. P.; Polito, L.; Bigini, P.; Sitia, G. Functional Polarization of Liver Macrophages by Glyco Gold Nanoparticles. *Adv. Sci.* **2025**, *12* (16), No. 2407458, DOI: 10.1002/advs.202407458.

(3) Ruhoff, V. T.; Arastoo, M. R.; Moreno-Pescador, G.; Bendix, P. M. Biological Applications of Thermoplasmonics. *Nano Lett.* **2024**, *24* (3), 777−789.

(4) Kohout, C.; Santi, C.; Polito, L. Anisotropic Gold Nanoparticles in Biomedical Applications. *Int. J. Mol. Sci.* **2018**, *19* (11), No. 3385.

(5) Eker, F.; Akdaşçi, E.; Duman, H.; Bechelany, M.; Karav, S. Gold Nanoparticles in Nanomedicine: Unique Properties and Therapeutic Potential. *Nanomaterials* **2024**, *14* (22), No. 1854.

(6) Cardellini, J.; Surpi, A.; Muzzi, B.; Pacciani, V.; Innocenti, C.; Sangregorio, C.; Dediu, V. A.; Montis, C.; Berti, D. Magnetic−Plasmonic Nanoscale Liposomes with Tunable Optical and Magnetic Properties for Combined Multimodal Imaging and Drug Delivery. *ACS Appl. Nano Mater.* **2024**, *7* (4), 3668−3678.

(7) Veloso, S. R. S.; Gomes, V.; Mendes, S. L. F.; Hilliou, L.; Pereira, R. B.; Pereira, D. M.; Coutinho, P. J. G.; Ferreira, P. M. T.; Correa-Duarte, M. A.; Castanheira, E. M. S. Plasmonic Lipogels: Driving Co-Assembly of Composites with Peptide-Based Gels for Controlled Drug Release. *Soft Matter* **2022**, *18* (44), 8384−8397.

(8) Won, J. E.; Wi, T. I.; Lee, C. M.; Lee, J. H.; Kang, T. H.; Lee, J.-W.; Shin, B. C.; Lee, Y.; Park, Y.-M.; Han, H. D. NIR Irradiation-Controlled Drug Release Utilizing Injectable Hydrogels Containing Gold-Labeled Liposomes for the Treatment of Melanoma Cancer. *Acta Biomater.* **2021**, *136*, 508−518.

(9) Molinelli, A.; Schirato, A.; Moretti, L.; Della Valle, G.; Maiuri, M.; Rossi, F. Last Advances on Hydrogel Nanoparticles Composites in Medicine: An Overview with Focus on Gold Nanoparticles. *ChemNanoMat* **2024**, *10* (6), No. e202300584, DOI: 10.1002/cnma.202300584.

(10) Roshanbinfar, K.; Kolesnik-Gray, M.; Angeloni, M.; Schruefer, S.; Fiedler, M.; Schubert, D. W.; Ferrazzi, F.; Krstic, V.; Engel, F. B. Collagen Hydrogel Containing Polyethylenimine-Gold Nanoparticles for Drug Release and Enhanced Beating Properties of Engineered Cardiac Tissues. *Adv. Healthc. Mater.* **2023**, *12* (20), No. 2202408, DOI: 10.1002/adhm.202202408.

(11) Correa, S.; Grosskopf, A. K.; Klich, J. H.; Lopez Hernandez, H.; Appel, E. A. Injectable Liposome-Based Supramolecular Hydrogels for the Programmable Release of Multiple Protein Drugs. *Matter* **2022**, *5* (6), 1816−1838.

(12) Lacroce, E.; Nunziata, G.; Cianniello, F.; Limiti, E.; Rainer, A.; Vangosa, F. B.; Sacchetti, A.; Sponchioni, M.; Rossi, F. Amphiphilic PH-Responsive Core-Shell Nanoparticles Can Increase the Perform-

ances of Cellulose-Based Drug Delivery Systems. *Int. J. Biol. Macromol.* **2024**, *283*, No. 137659.
(13) Barbieri, V.; González Colsa, J.; Matias, D.; Duro Castano, A.; Thapa, A.; Ruiz-Pérez, L.; Albella, P.; Volpe, G.; Battaglia, G. Thermoplasmonic Polymersome Membranes by *In Situ* Synthesis. *ACS Nano* **2025**, *19* (16), 15331−15344.
(14) Lacroce, E.; Bianchi, L.; Polito, L.; Korganbayev, S.; Molinelli, A.; Sacchetti, A.; Saccomandi, P.; Rossi, F. On the Role of Polymeric Hydrogels in the Thermal Response of Gold Nanorods under NIR Laser Irradiation. *Nanoscale Adv.* **2023**, *5*, 6870−6879.
(15) Egorikhina, M. N.; Timofeeva, L. B.; Linkova, D. D.; Rubtsova, Y. P.; Bugrova, M. L.; Charykova, I. N.; Ryabkov, M. G.; Kobyakova, I. I.; Farafontova, E. A.; Aleynik, D. Y. Biocompatibility Study of Hydrogel Biopolymer Scaffold with Encapsulated Mesenchymal Stem Cells. *Polymers* **2023**, *15* (6), No. 1337.
(16) Giorgi, Z.; Veneruso, V.; Petillo, E.; Veglianese, P.; Perale, G.; Rossi, F. Biomaterials and Cell Therapy Combination in Central Nervous System Treatments. *ACS Appl. Bio Mater.* **2024**, *7* (1), 80−98.
(17) Lavrador, P.; Esteves, M. R.; Gaspar, V. M.; Mano, J. F.; Lavrador, P.; Esteves, M. R.; Gaspar, V. M.; Mano, J. F. Stimuli-Responsive Nanocomposite Hydrogels for Biomedical Applications. *Adv. Funct. Mater.* **2021**, *31* (8), No. 2005941.
(18) García-Astrain, C.; Lenzi, E.; Jimenez de Aberasturi, D.; Henriksen-Lacey, M.; Binelli, M. R.; Liz-Marzán, L. M. 3D-Printed Biocompatible Scaffolds with Built-In Nanoplasmonic Sensors. *Adv. Funct. Mater.* **2020**, *30* (45), No. 2005407, DOI: 10.1002/adfm.202005407.
(19) Ojea-Jiménez, I.; Bastús, N. G.; Puntes, V. Influence of the Sequence of the Reagents Addition in the Citrate-Mediated Synthesis of Gold Nanoparticles. *J. Phys. Chem. C* **2011**, *115* (32), 15752−15757.
(20) Schulz, F.; Homolka, T.; Bastús, N. G.; Puntes, V.; Weller, H.; Vossmeyer, T. Little Adjustments Significantly Improve the Turkevich Synthesis of Gold Nanoparticles. *Langmuir* **2014**, *30* (35), 10779−10784.
(21) Kettemann, F.; Birnbaum, A.; Witte, S.; Wuithschick, M.; Pinna, N.; Kraehnert, R.; Rademann, K.; Polte, J. Missing Piece of the Mechanism of the Turkevich Method: The Critical Role of Citrate Protonation. *Chem. Mater.* **2016**, *28* (11), 4072−4081.
(22) Amina, S. J.; Guo, B. A. Review on the Synthesis and Functionalization of Gold Nanoparticles as a Drug Delivery Vehicle. *Int. J. Nanomed.* **2020**, *15*, 9823−9857.
(23) Bastús, N. G.; Comenge, J.; Puntes, V. Kinetically Controlled Seeded Growth Synthesis of Citrate-Stabilized Gold Nanoparticles of up to 200 Nm: Size Focusing versus Ostwald Ripening. *Langmuir* **2011**, *27* (17), 11098−11105.
(24) Piella, J.; Bastús, N. G.; Puntes, V. Size-Controlled Synthesis of Sub-10-Nanometer Citrate-Stabilized Gold Nanoparticles and Related Optical Properties. *Chem. Mater.* **2016**, *28* (4), 1066−1075.
(25) Bartosewicz, B.; Bujno, K.; Liszewska, M.; Budner, B.; Bazarnik, P.; Płociński, T.; Jankiewicz, B. J. Effect of Citrate Substitution by Various α-Hydroxycarboxylate Anions on Properties of Gold Nanoparticles Synthesized by Turkevich Method. *Colloids Surf., A* **2018**, *549*, 25−33.
(26) Mironov, I. V.; Kharlamova, V. Yu. Synthesis of Gold Nanoparticles in Aqueous Solutions Not Containing Additional Interfering Components Using Sulfite Method: The Effect of Thiol-Containing Acid Additives. *Gold Bull.* **2021**, *54* (1), 37−44.
(27) Ahmed, S.; Baijal, G.; Somashekar, R.; Iyer, S.; Nayak, V. One Pot Synthesis of Pegylated Bimetallic Gold− Silver Nanoparticles for Imaging and Radiosensitization of Oral Cancers. *Int. J. Nanomed.* **2021**, *16*, 7103−7121.
(28) Dolya, N.; Rojas, O.; Kosmella, S.; Tiersch, B.; Koetz, J.; Kudaibergenov, S. One-Pot" in Situ Formation of Gold Nanoparticles within Poly(Acrylamide) Hydrogels. *Macromol. Chem. Phys.* **2013**, *214* (10), 1114−1121.
(29) Das, R.; Das, D.; Ghosh, P.; Dhara, S.; Panda, A. B.; Pal, S. Development and Application of a Nanocomposite Derived from Crosslinked HPMC and Au Nanoparticles for Colon Targeted Drug Delivery. *RSC Adv.* **2015**, *5* (35), 27481−27490.
(30) Pham, Q. T.; Ngo, G. L.; Nguyen, X. A.; Nguyen, C. T.; Ledoux-Rak, I.; Lai, N. D. Direct Synthesis of Gold Nanoparticles in Polymer Matrix. *Polymers* **2023**, *15* (1), No. 16.
(31) Wagner, M.; Krieger, A.; Gröhn, F. Gold Nanoparticles in Disulfide Based Polymer Matrices: Size, Structure and Responsivity. *Macromol. Chem. Phys.* **2024**, *225* (4), No. 2300342, DOI: 10.1002/macp.202300342.
(32) Figat, A. M.; Bartosewicz, B.; Liszewska, M.; Budner, B.; Norek, M.; Jankiewicz, B. J. α-Amino Acids as Reducing and Capping Agents in Gold Nanoparticles Synthesis Using the Turkevich Method. *Langmuir* **2023**, *39* (25), 8646−8657.
(33) Marques, M. S.; Zepon, K. M.; Heckler, J. M.; Morisso, F. D. P.; da Silva Paula, M. M.; Kanis, L. A. One-Pot Synthesis of Gold Nanoparticles Embedded in Polysaccharide-Based Hydrogel: Physical-Chemical Characterization and Feasibility for Large-Scale Production. *Int. J. Biol. Macromol.* **2019**, *124*, 838−845.
(34) Assad, N.; Laila, M. B.; Hassan, M. N. U.; ur Rehman, M. F.; Ali, L.; Mustaqeem, M.; Ullah, B.; Khan, M. N.; Iqbal, M.; Ercişli, S.; Alarfaj, A. A.; Ansari, M. J.; Malik, T. Eco-Friendly Synthesis of Gold Nanoparticles Using Equisetum Diffusum D. Don. with Broad-Spectrum Antibacterial, Anticancer, Antidiabetic, and Antioxidant Potentials. *Sci. Rep.* **2025**, *15* (1), No. 19246.
(35) Parveen, R.; Tremiliosi-Filho, G. A Step Ahead towards the Green Synthesis of Monodisperse Gold Nanoparticles: The Use of Crude Glycerol as a Greener and Low-Cost Reducing Agent. *RSC Adv.* **2016**, *6* (97), 95210−95219.
(36) Rasmussen, D. R.; Nielsen, M. F.; Quinson, J. Room Temperature Surfactant-Free Synthesis of Gold Nanoparticles in Alkaline Ethylene Glycol. *Chemistry* **2023**, *5* (2), 900−911.
(37) Li, R.; Wang, Z.; Gu, X.; Chen, C.; Zhang, Y.; Hu, D. Study on the Assembly Structure Variation of Cetyltrimethylammonium Bromide on the Surface of Gold Nanoparticles. *ACS Omega* **2020**, *5* (10), 4943−4952.
(38) Suchomel, P.; Kvitek, L.; Prucek, R.; Panacek, A.; Halder, A.; Vajda, S.; Zboril, R. Simple Size-Controlled Synthesis of Au Nanoparticles and Their Size-Dependent Catalytic Activity. *Sci. Rep.* **2018**, *8* (1), No. 4589.
(39) Andersen, K. J.; Varga, M.; Smolska, A.; Nordhal, G.; Jensen, J. H.; Moreno, R.; Bøjesen, E. D.; Anker, A. S.; Quinson, J. Positive Thinking: Countercation Effects in Colloidal Syntheses of Gold Nanoparticles. *Nano Lett.* **2025**, *25* (42), 15436−15442.
(40) Vinnacombe-Willson, G. A.; Conti, Y.; Stefancu, A.; Weiss, P. S.; Cortés, E.; Scarabelli, L. Direct Bottom-Up In Situ Growth: A Paradigm Shift for Studies in Wet-Chemical Synthesis of Gold Nanoparticles. *Chem. Rev.* **2023**, *123* (13), 8488−8529.
(41) Vinnacombe-Willson, G. A.; Núñez-Martínez, M.; Herrero-Ruiz, A.; Bevilacqua, F.; Pazos, R.; Troncoso-Afonso, L.; Gallego-González, M.; Scarabelli, L.; Liz-Marzán, L. M. Plasmonic-Hydrogel Hybrid Biomaterials Via In Situ Seeded Growth. *Angew. Chem.* **2025**, *64* (25), No. e202501854, DOI: 10.1002/anie.202501854.
(42) Faoucher, E.; Nativo, P.; Black, K.; Claridge, J. B.; Gass, M.; Romani, S.; Bleloch, A. L.; Brust, M. In Situ Preparation of Network Forming Gold Nanoparticles in Agarose Hydrogels. *Chem. Commun.* **2009**, No. 43, 6661−6663.
(43) Fortuni, B.; Fujita, Y.; Ricci, M.; Inose, T.; Aubert, R.; Lu, G.; Hutchison, J. A.; Hofkens, J.; Latterini, L.; Uji-i, H. A Novel Method for in Situ Synthesis of SERS-Active Gold Nanostars on Polydimethylsiloxane Film. *Chem. Commun.* **2017**, *53* (37), 5121−5124.
(44) Vinnacombe-Willson, G. A.; García-Astrain, C.; Troncoso-Afonso, L.; Wagner, M.; Langer, J.; González-Callejo, P.; Di Silvio, D.; Liz-Marzán, L. M. Growing Gold Nanostars on 3D Hydrogel Surfaces. *Chem. Mater.* **2024**, *36* (10), 5192−5203.
(45) Nezhad-Mokhtari, P.; Akrami-Hasan-Kohal, M.; Ghorbani, M. An Injectable Chitosan-Based Hydrogel Scaffold Containing Gold Nanoparticles for Tissue Engineering Applications. *Int. J. Biol. Macromol.* **2020**, *154*, 198−205.

https://doi.org/10.1021/acsanm.5c05814
ACS Appl. Nano Mater. 2026, 9, 5067−5083

(46) Marić, I.; Vujičić, N. Š.; Pustak, A.; Gotić, M.; Jurkin, T. One-Step Synthesis of Poly(Ethylene Oxide)/Gold Nanocomposite Hydrogels and Suspensions Using Gamma-Irradiation. *Radiat. Phys. Chem.* **2020**, *170*, No. 108657.
(47) Jagankar, D.; Manohar, G.; Srivastava, P.; Maity, C. Facile Room-Temperature One-Pot Synthesis of a Gold Nanoparticle-Embedded Hydrogel for Recyclable Dye Degradation and Antimicrobial Applications. *Environ. Sci. Nano* **2026**, *13*, No. 861.
(48) Mondo, G. B.; da Silva Ribeiro, C. A.; Schlüter, L. G.; Bellettini, I. C.; Pavlova, E.; Giacomelli, F. C. One-Pot Bottom-up Synthesis of Gold Nanoparticles Mediated by Nitrogen-Containing Polymers: The Role of Chain Features and Environmental Conditions. *Colloids Surf., A* **2024**, *703*, No. 135116.
(49) Hu, S.; Huang, P.-J. J.; Wang, J.; Liu, J. Dissecting the Effect of Salt for More Sensitive Label-Free Colorimetric Detection of DNA Using Gold Nanoparticles. *Anal. Chem.* **2020**, *92* (19), 13354−13360.
(50) Luo, C.; Zhang, Y.; Zeng, X.; Zeng, Y.; Wang, Y. The Role of Poly(Ethylene Glycol) in the Formation of Silver Nanoparticles. *J. Colloid Interface Sci.* **2005**, *288* (2), 444−448.
(51) Niţică, t.; Moldovan, A. I.; Toma, V.; Moldovan, C. S.; Berindan-Neagoe, I.; Ştiufiuc, G.; Lucaciu, C. M.; Ştiufiuc, R. PEGylated Gold Nanoparticles with Interesting Plasmonic Properties Synthesized Using an Original, Rapid, and Easy-to-Implement Procedure. *J. Nanomater.* **2018**, *2018*, No. 5954028.
(52) Giorgi, Z.; Veneruso, V.; Petillo, E.; Vangosa, F. B.; Nogueira, L. P.; Haugen, H. J.; Veglianese, P.; Perale, G.; Rossi, F. Exploring the Role of Aqueous Buffered Saline Solutions on the Macroscopic Properties of PEG/Carbomer/Agarose Hydrogels. *Macromol. Biosci.* **2025**, *25*, No. 2500073, DOI: 10.1002/mabi.202500073.
(53) Stiufiuc, R.; Iacovita, C.; Nicoara, R.; Stiufiuc, G.; Florea, A.; Achim, M.; Lucaciu, C. M. One-Step Synthesis of PEGylated Gold Nanoparticles with Tunable Surface Charge. *J. Nanomater.* **2013**, *2013*, No. 146031, DOI: 10.1155/2013/146031.
(54) Fiévet, F.; Ammar-Merah, S.; Brayner, R.; Chau, F.; Giraud, M.; Mammeri, F.; Peron, J.; Piquemal, J.-Y.; Sicard, L.; Viau, G. The Polyol Process: A Unique Method for Easy Access to Metal Nanoparticles with Tailored Sizes, Shapes and Compositions. *Chem. Soc. Rev.* **2018**, *47* (14), 5187−5233.
(55) Rossi, F.; Perale, G.; Masi, M. Biological Buffered Saline Solution as Solvent in Agar-Carbomer Hydrogel Synthesis. *Chem. Pap.* **2010**, *64* (5), 573−578, DOI: 10.2478/s11696-010-0052-4.
(56) Rossi, F.; Santoro, M.; Casalini, T.; Veglianese, P.; Masi, M.; Perale, G. Characterization and Degradation Behavior of Agar−Carbomer Based Hydrogels for Drug Delivery Applications: Solute Effect. *Int. J. Mol. Sci.* **2011**, *12* (6), 3394−3408.
(57) Omping, J.; Unabia, R.; Reazo, R. L.; Lapening, M.; Lumod, R.; Ruda, A.; Rivera, R. B.; Sayson, N. L.; Latayada, F.; Capangpangan, R.; Dumancas, G.; Malaluan, R.; Lubguban, A.; Petalcorin, G.; Alguno, A. Facile Synthesis of PEGylated Gold Nanoparticles for Enhanced Colorimetric Detection of Histamine. *ACS Omega* **2024**, *9* (12), 14269−14278.
(58) Panáček, A.; Prucek, R.; Hrbáč, J.; Nevečná, T.; Šteffková, J.; Zbořil, R.; Kvítek, L. Polyacrylate-Assisted Size Control of Silver Nanoparticles and Their Catalytic Activity. *Chem. Mater.* **2014**, *26* (3), 1332−1339.
(59) Tang, J.; Fu, X.; Ou, Q.; Gao, K.; Man, S.-Q.; Guo, J.; Liu, Y. Hydroxide Assisted Synthesis of Monodisperse and Biocompatible Gold Nanoparticles with Dextran. *Mater. Sci. Eng., C* **2018**, *93*, 759−767.
(60) Wang, X.; Wang, C.; Wang, R.; Gu, D.; Chen, F. Gold Nanostructures Growth in HAuCl4-CTAB-NaOH Aqueous Solution without Any Reducing Agent. *J. Cryst. Growth* **2023**, *602*, No. 126991.
(61) Unnikrishnan, A.; Alexander, L. K. The Concentration-Dependent Effect of NaOH on Graphene Oxide: Revisited as a Reducing Agent. *J. Phys. Chem. Solids* **2024**, *190*, No. 111978.
(62) Caron, I.; Rossi, F.; Papa, S.; Aloe, R.; Sculco, M.; Mauri, E.; Sacchetti, A.; Erba, E.; Panini, N.; Parazzi, V.; Barilani, M.; Forloni, G.; Perale, G.; Lazzari, L.; Veglianese, P. A New Three Dimensional Biomimetic Hydrogel to Deliver Factors Secreted by Human Mesenchymal Stem Cells in Spinal Cord Injury. *Biomaterials* **2016**, *75*, 135−147.
(63) Mauri, E.; Sacchetti, A.; Vicario, N.; Peruzzotti-Jametti, L.; Rossi, F.; Pluchino, S. Evaluation of RGD Functionalization in Hybrid Hydrogels as 3D Neural Stem Cell Culture Systems. *Biomater. Sci.* **2018**, *6* (3), 501−510.
(64) Molinelli, A.; Bianchi, L.; Lacroce, E.; Giorgi, Z.; Polito, L.; De Luigi, A.; Lopriore, F.; Briatico Vangosa, F.; Bigini, P.; Saccomandi, P.; Rossi, F. Design and Characterization of Gold Nanorod Hyaluronic Acid Hydrogel Nanocomposites for NIR Photothermally Assisted Drug Delivery. *Gels* **2026**, *12* (1), No. 88.

https://doi.org/10.1021/acsanm.5c05814
ACS Appl. Nano Mater. 2026, 9, 5067−5083